Precambrian Research 436 (2026) 108040

Contents lists available at ScienceDirect

Precambrian Research

journal homepage: www.elsevier.com/locate/precamres

Research Paper

# Paleoproterozoic tectonic evolution of the Dunhuang Block, eastern Tarim: insights from geochronology and petrogenesis of *meta*-igneous rocks

Xiang Ren [a], Baoping Gan [a,*], Inna Safonova [a,*], Faqiao Li [b], Qingfei Sun [a], Hongrui Xu [a]

[a] Faculty of Geosciences and Engineering, Southwest Jiaotong University, Chengdu 611756, China
[b] Institute of Mineral Resources, Chinese Academy of Geological Sciences, Beijing 100037, China

ARTICLE INFO

*Keywords:*
Columbia supercontinent
Paleoproterozoic
Dunhuang Block
Tectonothermal events
Amphibolite and granitic gneiss

ABSTRACT

Identification of Paleoproterozoic tectonothermal events in ancient continental blocks is crucial for understanding the history of the Columbia supercontinent. The Dunhuang Block is located east of the Tarim Craton and it keeps archives of multiple events of Paleoproterozoic magmatism and metamorphism. It represents an excellent window to understand tectonic relationships between the Dunhuang Block and adjacent Tarim and North China cratons and to trace its tectonic evolution during the assembly of Columbia. In this paper, we present first data on zircon and apatite U-Pb geochronology, whole-rock geochemistry and Hf-in-zircon isotopes from newly discovered Paleoproterozoic *meta*-igneous rocks, amphibolite and granitic gneiss, that are exposed in the Dongshuigou area of the Dunhuang Block. Amphibolite and granitic gneiss yielded similar U-Pb zircon ages of crystallization of igneous protoliths, ~2.02 and ~ 2.04 Ga, respectively. Apatite U-Pb dating of both rocks indicates a late Paleozoic tectonothermal event, probably, superimposed metamorphism at 391–380 Ma. The amphibolites are enriched in light rare earth element (LREE) and large ion lithophile elements (LILE), depleted in high field strength elements (HFSE) and possess depleted Hf-in-zircon isotope characteristics ($\varepsilon_{Hf}(t) = +0.71$ to $+ 4.93$); their igneous mafic protoliths were possibly derived by low-degree melting of an enriched mantle wedge source. The granitic gneisses possess geochemical affinities to TTG: $SiO_2$ of 73.03 to 78.05 wt%, low $K_2O/Na_2O$ ratios (0.17–0.22 wt%), enriched LREE, depleted heavy REE, and high Sr/Y (57–82). Such geochemical characteristics and the $\varepsilon_{Hf}(t)$ values spanning $-2.7$ to $+ 1.2$ suggest that the granitic gneisses could be derived by melting of TTG-type igneous protoliths triggered by intrusion of hot mantle-derived magmas. The protoliths of both types of *meta*-igneous rocks were probably emplaced in an active continental margin setting. The new data from the Dunhuang Block accord well with previous data from other Neoarchean-Paleoproterozoic magmatic and metamorphic rocks of the whole Dunhuang-Tarim region suggesting similar and nearly synchronous tectonic evolution: the Dunhuang Block approached northern Tarim during oceanic subduction at ca. 2.0–1.90 Ga and then experienced collisional orogeny at ca. 1.85–1.82 Ga. The Dunhuang and Tarim blocks could be both involved into the assembly of the Columbia supercontinent at ca. 2.1–1.8 Ga.

## 1. Introduction

In the Earth's geological history nearly all continental blocks periodically assembled to form huge landmasses-supercontinents (Condie, 2003b, 2011; Murphy and Nance, 2013; Nance et al., 2014; Li et al., 2016a; Mitchell et al., 2021). An early event of supercontinent formation happened during the Paleoproterozoic era, when the Columbia (or Nuna) supercontinent assembled (e.g., Rogers and Santosh, 2002; Zhao et al., 2002, 2004; Meert and Santosh, 2017; Evans et al., 2011). The most compelling piece of evidence for the Columbia supercontinent comes from a global-scale collisional orogeny at ca. 2.1–1.8 Ga (e.g., Zhao et al., 2002, 2004) that resulted in amalgamation of almost all Earth's major continental blocks to form the Columbia supercontinent (e.g., Rogers and Santosh, 2002). Therefore, identification of Paleoproterozoic magmatic and metamorphic archives related to orogeny (tectonothermal events) in space and time is crucial to understand which Precambrian landmasses participated in the assembly of the Columbia supercontinent and their tectonic affinity with other continental blocks in the configuration of Columbia, in particular, in respect of relatively small blocks.

* Corresponding authors.
*E-mail addresses:* baoping@swjtu.edu.cn (B. Gan), inna03-64@mail.ru (I. Safonova).

https://doi.org/10.1016/j.precamres.2026.108040
Received 24 July 2025; Received in revised form 1 November 2025; Accepted 3 February 2026
Available online 12 February 2026

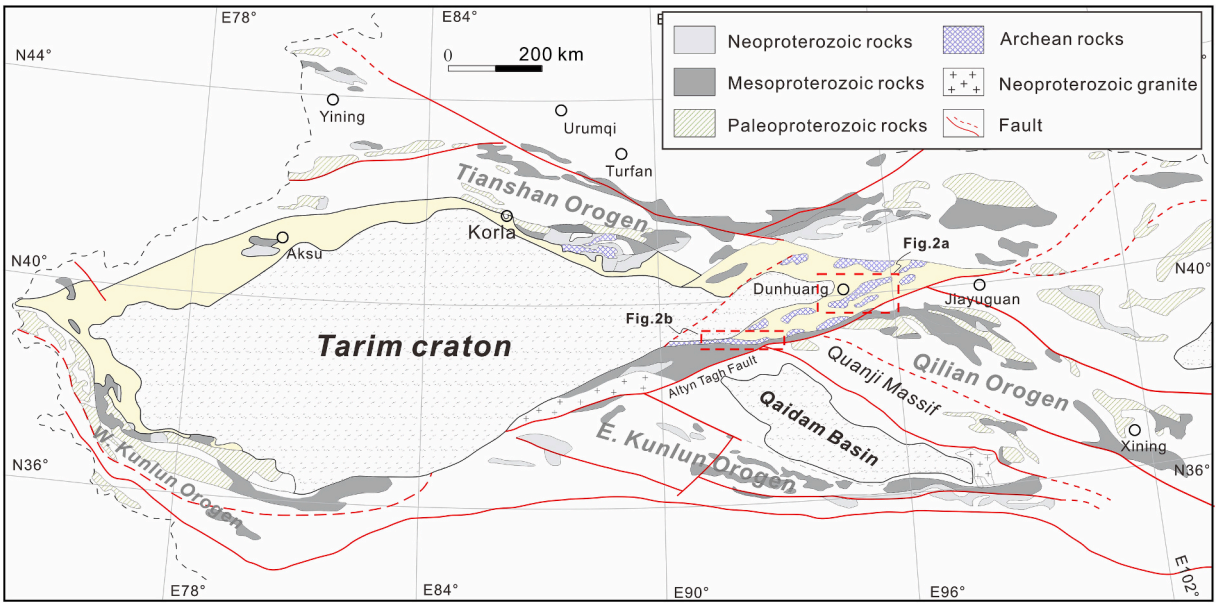


**Fig. 1.** Tectonic scheme of the Tarim Craton and surrounding orogens (modified from Wu et al., 2019).

The major Precambrian blocks of China are North China Craton (NCC), Tarim Craton (TC) and South China Craton (SCC) that all were argued to experience Paleoproterozoic orogeny related to the assembly of the Columbia supercontinent (e.g., Zhao et al., 2003, 2005; Zhao and Cawood, 2012; Zhai and Liu 2003; Zhai and Santosh, 2011). Among three cratons, the NCC has been better studied: its geological structure includes three Paleoproterozoic collisional belts and its tectonic evolution traces both the assembly and the breakup of the Columbia supercontinent (e.g., Zhao et al., 2011). The Paleoproterozoic collisional belts of the NCC are Khondalite, Jiao-Liao-Ji and Trans-North China belts. The ~ 1.95 Ga Khondalite Belt marks the amalgamation of the Yinshan and Ordos blocks to form the Western Block of NCC (Zhao et al., 2002, 2005; Zhai et al., 2010; Zhai and Santosh, 2011). The ~ 1.9 Ga Jiao-Liao-Ji Belt in the Eastern Block, formed by subduction-collisional orogeny (Faure et al., 2004; Zhou et al., 2008; Zhao et al., 2011, 2012; Zhao and Zhai, 2013). The Trans-North China Orogen is dominated by ~ 1.85 Ga high-pressure metamorphic rocks and it resulted from the collision of the Eastern and Western blocks to form a single cratonic block during assembly of the Columbia supercontinent (e.g., Wilde et al., 2002; Guo et al., 2005; Liu et al., 2006; Wang et al., 2010; Zhao et al., 2011). The SCC also keeps numerous archives of Paleoproterozoic metamorphic and magmatic events related to the assembly Columbia (e.g., Zhang et al., 2006; Wu et al., 2009; Yin et al., 2013; Wang et al., 2014a; Guo et al., 2015; Li et al., 2016b). However, the Paleoproterozoic history of the TC and its surrounding terranes has been lesser understood as the craton is covered by thick Cenozoic sediments so that the Precambrian basement rocks are exposed only along its margins (Shu et al., 2011; Xin et al., 2011, 2013; Long et al., 2012; Ge et al., 2013a, 2013b, 2014; Xu et al., 2013). Two Paleoproterozoic orogenic belts have been reconstructed in the TC: the ca. 2.0–1.9 Ga South Tarim orogen and the ca. 1.9–1.8 Ga Northern Tarim orogen (Ge et al., 2013b, 2015). In this context, the Paleoproterozoic history TC has been parallelized with the Alxa Block of the NCC (Ge et al., 2015) and they both were considered to participate in the assembly of Columbia (e.g., Xu et al., 2013; Ge et al., 2015; Wu et al., 2019).

The Dunhuang Block is located in the eastern TC and it is bounded by the Alxa Block to the east (Fig. 1). The tectonic position of the Dunhuang Block in respect to the adjacent TC and NCC in Neoarchean-Paleoproterozoic time remains debatable. Based on an analysis of Neoarchean crustal growth, and Paleoproterozoic events of magmatism and metamorphism, the Dunhuang Block has been previously considered as a part of the TC (Mei et al., 1997; Meng et al., 2011; Long et al., 2014) or a westward extension of the NCC (Zhang et al., 2011, 2012b). Later, based on a comparison of regional Paleoproterozoic magmatic-metamorphic events, the TC including the Dunhuang Block was argued to be correlative to the Alxa Block of the NCC (Ge et al., 2015; Zhao et al., 2015b). Precambrian basement rocks are widely exposed in the Dunhuang Block and therefore provide a key to understand its tectonic relationships with surrounding continental blocks. During the past decade, numerous outcrops of Paleoproterozoic magmatic and metamorphic rocks have been reported in the Dunhuang Block (Fig. 2; Zhang et al., 2012b, 2013a; He et al., 2013; Zhao et al., 2015a, 2019b, 2020, 2022). Evidence for the Paleoproterozoic collision related tectonothermal events comes from ~ 1.85 Ga high-pressure granulites of the Shibaocheng area in the southern Dunhuang Block (Zhang et al., 2012b). The occurrence of 1.79–1.73 Ga A-type granites indicates that the Dunhuang Block experienced late Paleoproterozoic post-collisional magmatism (Yu et al., 2014; Gan et al., 2020). Those findings fit well the global-scale Paleoproterozoic orogenic events related to the assembly of the Columbia supercontinent (Zhao et al., 2002, 2004). Nevertheless, the Paleoproterozoic tectonic evolution of the Dunhuang Block prior to the ~ 1.85 Ga continental collision has not been well constrained yet. Therefore, identification of Paleoproterozoic tectonothermal events in the Dunhuang Block is of particular importance for understanding its tectonic relationships with neighboring continental blocks during the Paleoproterozoic and its tectonic position during the assembly of Columbia.

In this paper, we report new U-Pb zircon and apatite ages, whole-rock geochemical data and Hf-in-zircon isotope data from Paleoproterozoic amphibolites and granitic gneisses of the Dongshuigou area in the central part of the Dunhuang Block in order to determine the ages of their igneous protoliths and event of superimposed metamorphism, to reconstruct their petrogenesis and to discriminate tectonic settings. In addition, integration of new and previous geochronological data allows us to establish a succession of Neoarchean-Paleoproterozoic tectonothermal events as recorded in the Dunhuang Block, and to discuss its tectonic relationships with the NCC and TC and tectonic position during the assembly of the Columbia supercontinent.

## 2. Geological overview

The Dunhuang Block is situated at the eastern margin of the TC and it

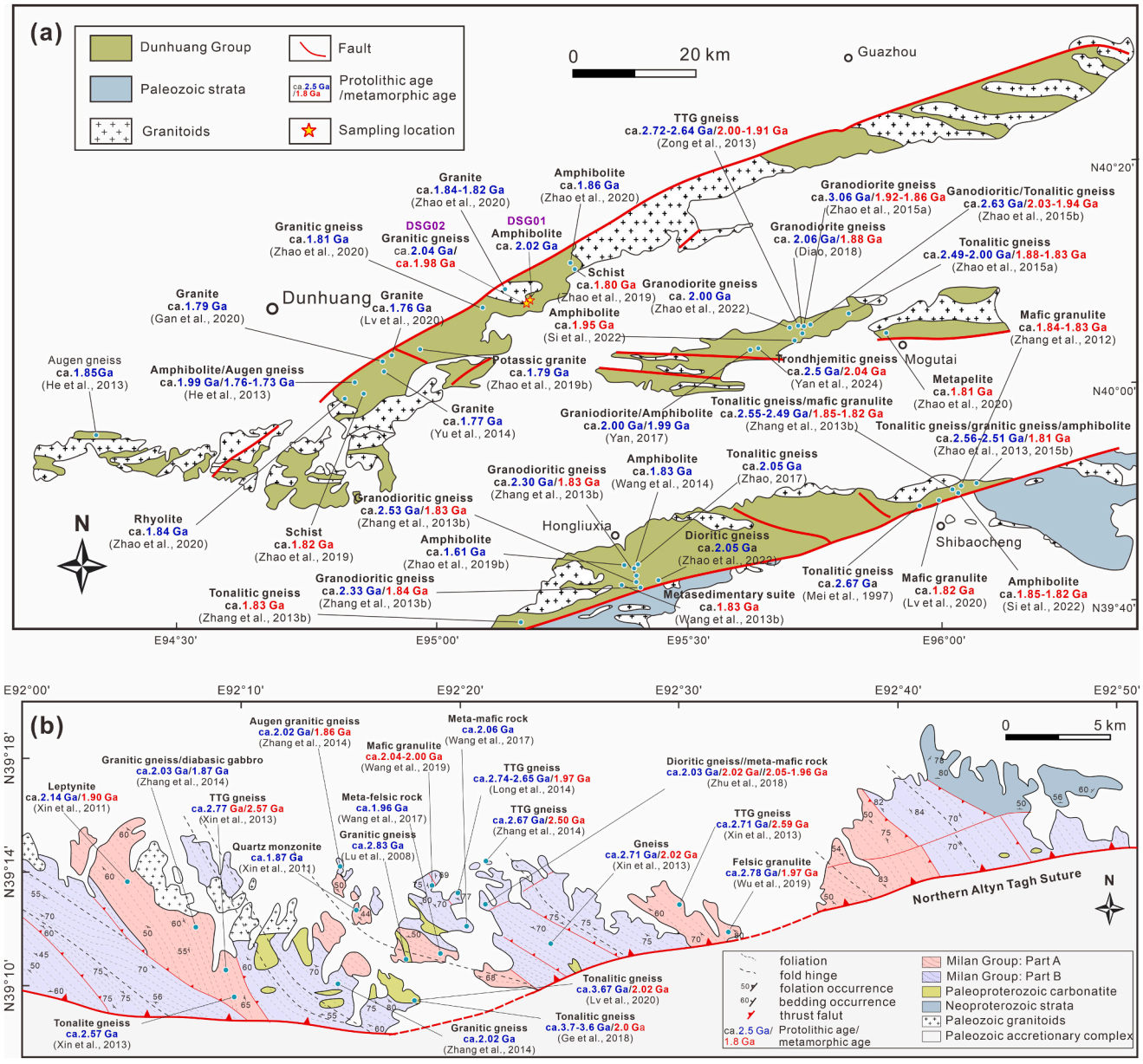


**Fig. 2.** Simplified geological map of the Dunhuang Block showing a spatial–temporal distribution of Neoarchean-Paleoproterozoic rocks. (a) Dunhuang region; (b) Aktashtagh region of north Altyn Tagh (modified from Ge et al., 2018).

occupies a triangular area, separated by the Qiemo-Xingxingxia fault from the main part of the TC to the west, and by the Altyn Tagh fault from the Alxa Block to the east and from the Qilian Orogen to the southeast (Fig. 1; Lu and Yuan, 2003; Lu et al., 2008). Previous studies show that the Dunhuang Block includes Precambrian basement rocks of the Aktashtagh region of northern Altyn Tagh and of the Dunhuang region. The oldest Archean-Paleoproterozoic rock formations that are exposed in the Dunhuang and Aktashtagh regions have been referred to as the Dunhuang and Milan groups, respectively (Mei et al., 1997; Lu et al., 2008; Meng et al., 2011; Zhu et al., 2018). Both groups consist of Neoarchean TTG (tonalite-trondhjemite-granodiorite) gneisses and Neoarchean-Paleoproterozoic metamorphosed supracrustal rocks, although they probably had different tectonic evolutions (Zhang et al., 2012b; Wu et al., 2019).

In the Dunhuang region, there are three NE-SW trending lithotectonic belts hosting Precambrian basement rocks and numerous outcrops of Paleozoic magmatic and metamorphic rocks (Fig. 2a). The Dunhuang Group is dominated by highly deformed TTG gneisses, amphibolites, mafic granulites and sedimentary supracrustal rocks. The TTG gneisses are exposed in the Gangou, Dongbatu, Shibaocheng, Langchaigou, Shuixiakou, and Hongliuxia areas in the central and southern parts of Dunhuang (Zhang et al., 2012b, 2013b, Zhao et al., 2013, 2015a; Zong et al., 2013). The ages of the protoliths of the TTG gneisses in Gangou, Dongbatu, Langchaigou, and Shibaocheng are 3.06 Ga, 2.6 Ga, 2.7–2.6 Ga, and 2.5 Ga respectively (Mei et al., 1997; Zong et al., 2013; Zhao et al., 2015a). In the Hongliuxia area, the protoliths of the TTG gneisses formed at 2.5–2.3 Ga and also underwent a superimposed event of 1.85–1.82 Ga high-pressure granulite facies metamorphism (Zhang et al., 2013b). The amphibolites in the Sanweishan, Hanxia and Yulinhe areas formed at 1.99–1.86 Ga (He et al., 2013; Zhao et al., 2020). The supracrustal rocks of the Dunhuang Group are garnet-kyanite schist, graphite-bearing marble, garnet amphibolite, gneiss and quartzite, plus a subordinate amount of metavolcanic rocks. In addition, there are also outcrops of 1.79–1.73 Ga A-type granites in the Sanweishan and Huoyanshan areas in the northern part of the Dunhuang region (Yu et al., 2014; Gan et al., 2020).

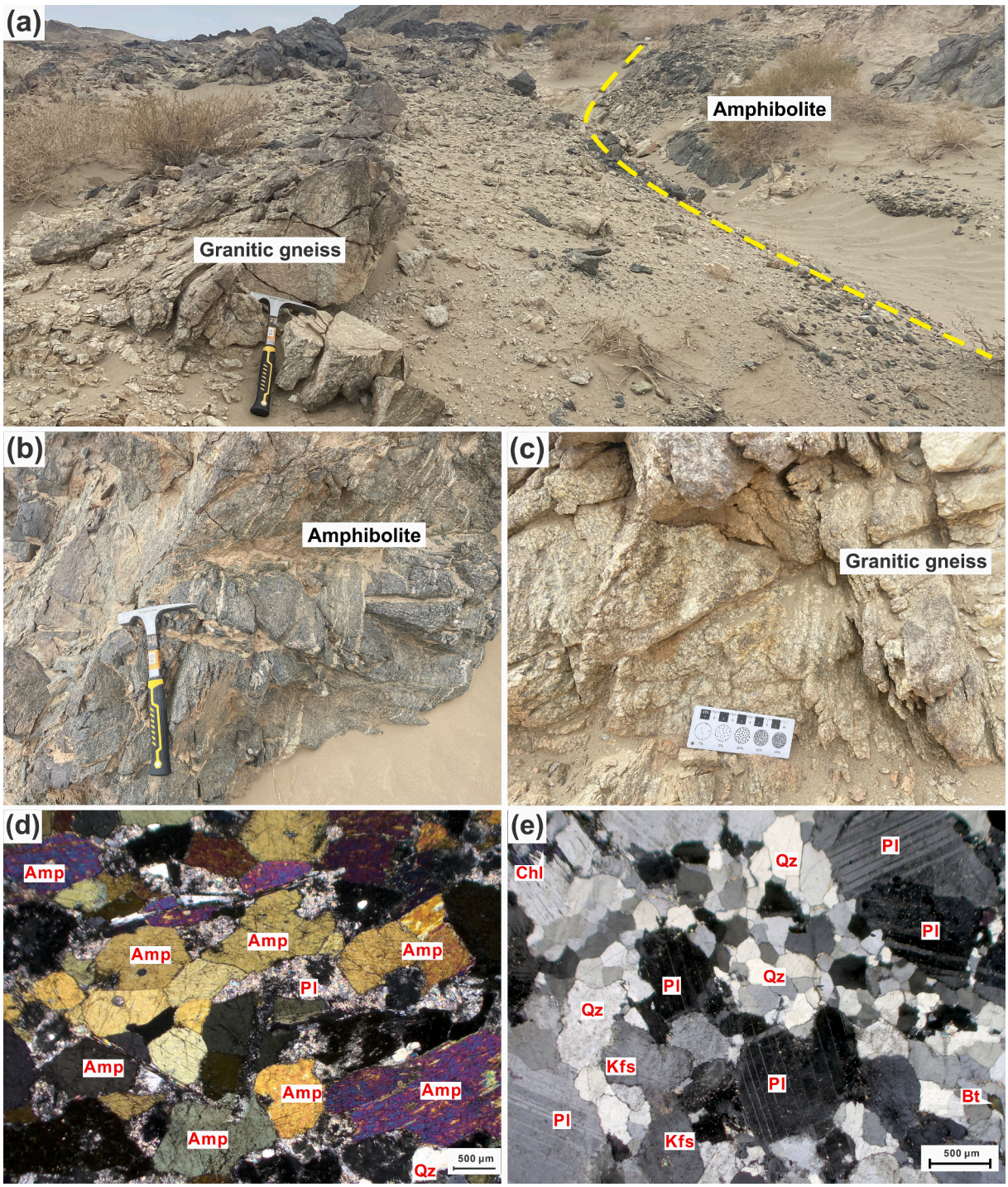


**Fig. 3.** Representative field photographs: (a) direct contact between amphibolite and granitic gneiss; (b) amphibolite cut by thin felsic dykes; (c) leucocratic granitic gneiss. (d and e) Photomicrographs of amphibolite and granitic gneiss showing typical mineral assemblages. Abbreviations are after Whitney and Evans (2010): Amp, amphibole, Pl, plagioclase, Qz, quartz, Kfs, K-feldspar, Bt, biotite, Chl, chlorite.

The Milan Group crops out in the Aktashtagh region of northern Altyn Tagh, and it is dominated by TTGs, monzogranitic and granitic gneisses (Fig. 2b; Lu, 2002; Liu et al., 2010), granulite, plus subordinate amphibolites (Lu, 2002; Lu and Yuan, 2003). The supracrustal metamorphic rocks, granulite, amphibolite, marble, metapelite and quartzite, look strongly deformed and often occur as enclaves within deformed felsic plutonic rocks (Che and Sun, 1996; Liu et al., 2010). The U-Pb zircon dating shows that the TTG gneisses formed at 2.8–2.5 Ga (Lu and Yuan, 2003; Lu et al., 2008; Liu et al., 2009; Xin et al., 2013; Long et al., 2014; Zhang et al., 2014), granitic gneiss, dioritic gneiss, and monzonite formed at 2.03–1.96 Ga (Zhang et al., 2014; Wang et al., 2017c; Zhu et al., 2018), and 1.87 Ga (Xin et al., 2011). In addition, a ~ 2.06 Ga amphibolite was found in the Aktashtagh region (Wang et al., 2017c). The age of the oldest zircon population of the Archean tonalitic gneiss that has been so far identified in the Aktashtagh region is ~ 3.7 Ga (Lu et al., 2008; Ge et al., 2018). The Neoarchean-Paleoproterozoic basement rocks were metamorphosed at 2.05–1.86 Ga (Xin et al., 2013; Zhang et al., 2014; Ge et al., 2018; Zhu et al., 2018; Wang et al., 2019; Wu et al., 2019; Lv et al., 2020). In addition, a volcanic rock yielded a SHRIMP U-Pb zircon age of 2592 Ma (Liu et al., 2009), and a

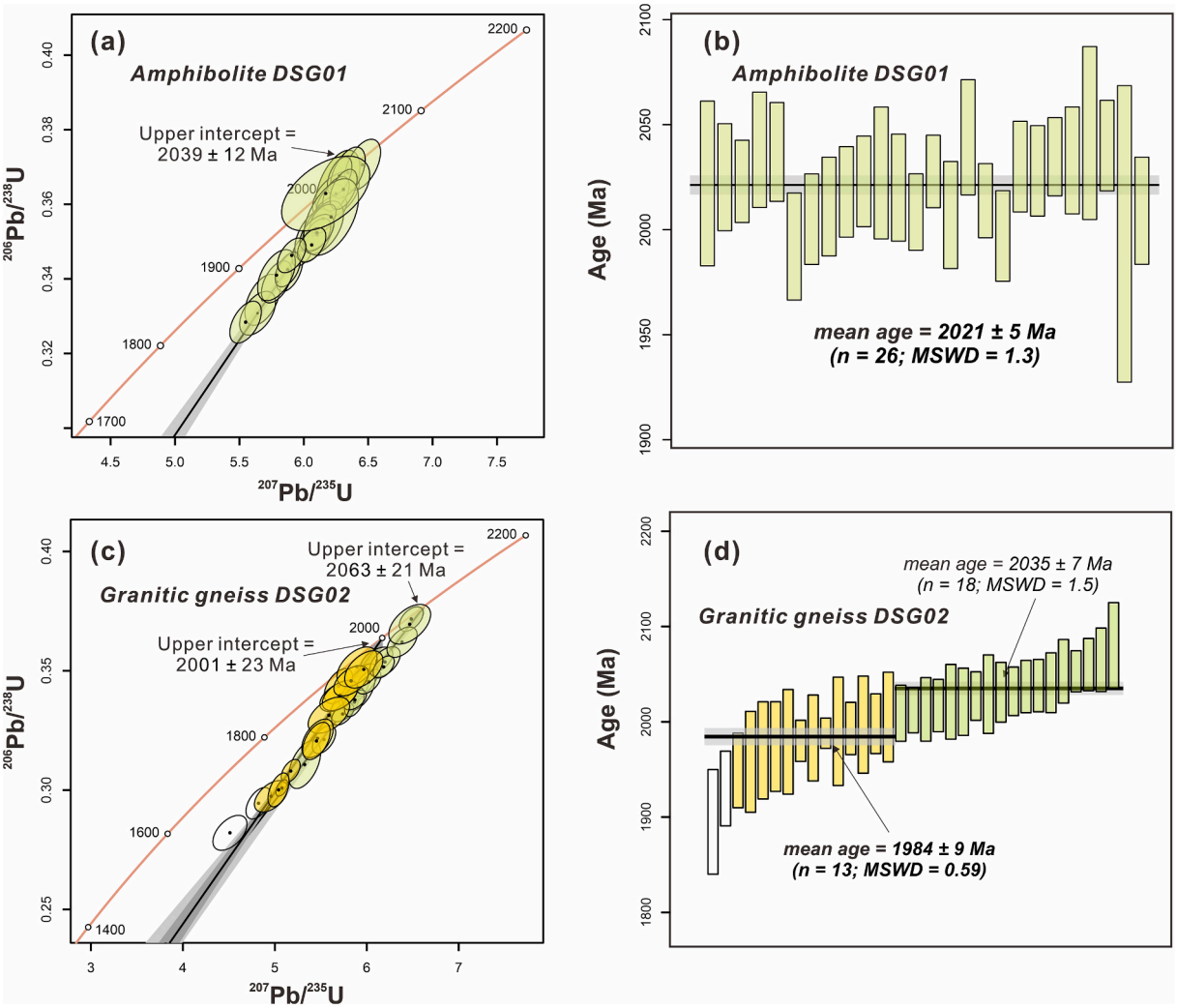


**Fig. 4.** (a, c) U-Pb zircon concordia diagrams. (b, d) Weighted mean U-Pb zircon ages. Light grey envelopes in panels b and d represent two standard deviations (2σ).

metasedimentary rock yielded $^{207}Pb/^{206}Pb$ detrital zircon ages in the range from 2884 Ma to 2339 Ma (Lu et al., 2008). However, there remains a deficiency in isotope age data from the supracrustal rocks of the Milan Group.

During the Paleozoic, the Dunhuang Block experienced several tectonothermal events: numerous granites with crystallization ages of 510 Ma, 440–400 Ma, 370–360 Ma and 330–310 Ma intruded the Precambrian basement rocks (Gan et al., 2024 and references therein). There are also variable high-grade metamorphosed rocks, eclogites, high-pressure granulites and amphibolites that occur as blocks, lenses or boudines surrounded by metaclastic rocks and marbles in the Hongliuxia and Mogutai areas. The age of metamorphism ranges from 440 to 350 Ma (He et al., 2014; Si et al., 2022; Wang et al., 2017a,b; Zong et al., 2012). The Paleozoic metamorphic rocks are typically characterized by clockwise P-T paths implying a collisional orogeny (He et al., 2014; Wang et al., 2017b; Zong et al., 2012).

## 3. Sampling and petrography

We collected Paleoproterozoic *meta*-igneous rocks in the southern Dongshuigou area that is located in the middle of a NEE-SWW-trending tectonic belt in the Dunhuang region (Fig. 2a). The Dongshuigou rock assemblage includes mica-quartz schists, biotite-plagioclase gneisses and gneissic granitoids that were intruded by the middle Devonian granites (389 Ma; Zhao et al., 2020), and 1.84–1.82 Ga granites that later experienced a late Devonian tectonothermal event (366 Ma; Zhao et al., 2020). The *meta*-igneous rocks under study are amphibolites and granitic gneisses of the Dunhuang Group (Fig. 2a). In outcrops, granitic gneisses have direct contacts with the amphibolites (Fig. 3a). The amphibolite (sample DSG01) that was analyzed for U-Pb age was collected at the southern edge of the Dongshuigou granitic pluton; it shows foliation and coherent leucocratic felsic veins (Fig. 3b). The amphibolite consists of amphibole (50–55%), plagioclase (30–35%), quartz (5–10%) and accessory zircon and apatite (Fig. 3d). Plagioclases are partly replaced by fine-grained sericite aggregates. The granitic gneiss dated for U-Pb geochronology (sample DSG02) shows a coarse-grained texture and weak foliation (Fig. 3c), and it consists mainly of quartz (30–35%), plagioclase (40–45%), K-feldspar (5–10%) and biotite (~5%) and accessory zircon and apatite (Fig. 3e). Biotite grains are aligned parallel to the foliation between the grains of feldspars.

## 4. Results

### 4.1. U-Pb zircon dating and Hf-in-zircon isotopes

The zircon grains from both samples, amphibolite DSG01 and granitic gneiss DSG02, are colorless, transparent with a size of 100–300 μm in length and aspect ratios of 1:1 to 2:1 (Fig. S1). The zircons from the amphibolite are sub-rounded and in CL images they are homogeneous, patched or banded internal structures with bright outermost rims

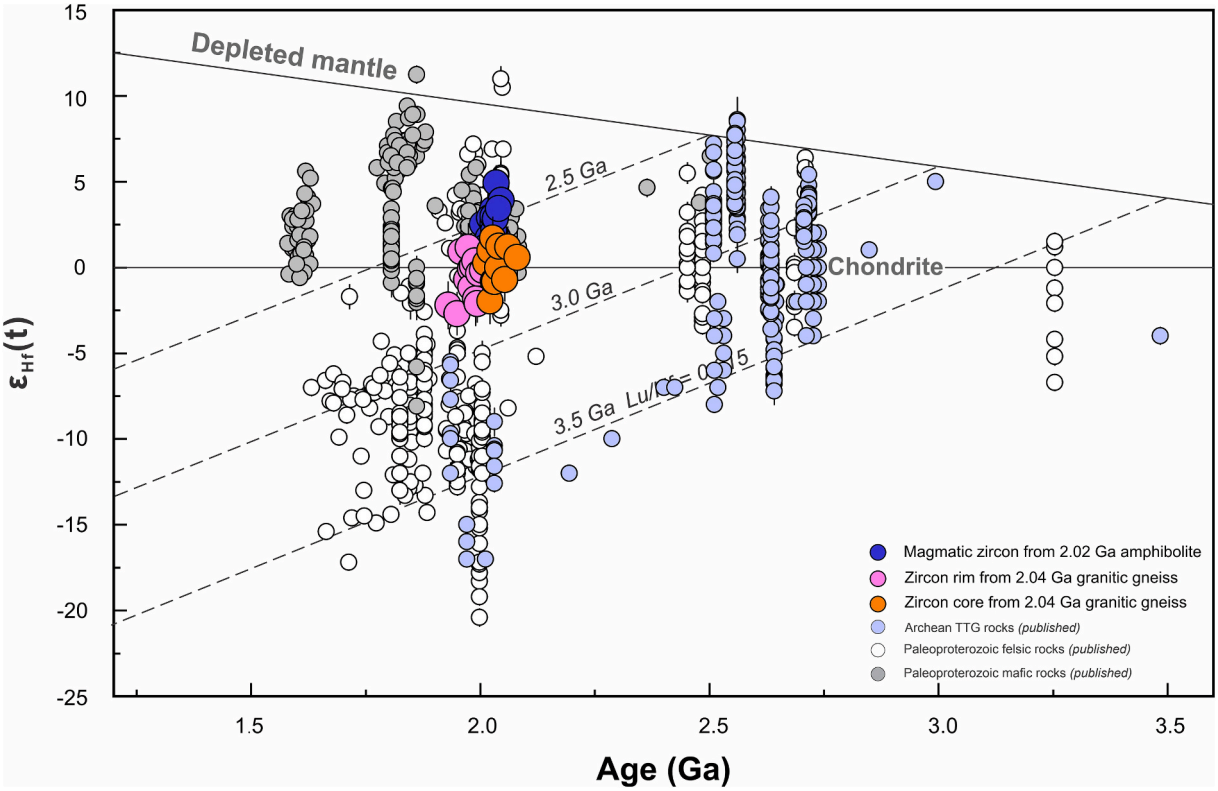


**Fig. 5.** Zircon age-corrected $\varepsilon_{Hf}(t)$ versus individual $^{207}Pb/^{206}Pb$ ages of amphibolite and granitic gneiss. Sources of $\varepsilon_{Hf}(t)$ data from other localities of Neoarchean-Paleoproterozoic rocks of Dunhuang Block: He et al. (2013); Zhao et al. (2013, 2015b, 2020, 2022); Zong et al. (2013); Long et al. (2014); Yu et al. (2014); Wang et al. (2014b, 2017c, 2020); Zhao (2017); Gan et al. (2020); Lv et al. (2020).

(Fig. S1) suggesting post-magmatic modification (Corfu et al., 2003). The zircons from the granitic gneiss are mostly euhedral to subhedral prismatic and a small fraction of those are stubby or oval (Fig. S1). In CL images, the zircons have clear core-rim structure and oscillatory zoning, or fir-tree and patchy zoning. There are also bright rims indicating later recrystallization or overgrowth (Fig. S1). There are also dark domains between the cores and the rims, and several cores have embayed margins probably due to dissolution.

Twenty-five zircons from amphibolite DSG01 were analyzed for geochronology. The zircons have relatively high Th/U ratios ranging from 0.44 to 1.34 (Fig. S1; Table S1), and REE patterns with positive Ce anomalies and negative Eu anomalies (Fig. S1; Table S2), both confirming their magmatic origin. The calculated $^{207}Pb/^{206}Pb$ ages range from 2046 Ma to 1992 Ma with a concordia upper intercept age at 2039 ± 12 Ma (Fig. 4a) and a weighted mean $^{207}Pb/^{206}Pb$ age of 2021 ± 5 Ma (MSWD = 1.3, n = 26) (Fig. 4b). Fifteen Lu-Hf isotopic ratios were measured in the dated zircons from the same sample. The values of $\varepsilon_{Hf}(t)$ were calculated based on the time of their crystallization. Hf isotope analyses yielded homogeneous $^{176}Hf/^{177}Hf$ ratios varying from 0.281576 to 0.281721 (Table S3), and consistently positive $\varepsilon_{Hf}(t)$ values between + 0.71 and + 4.93 (Fig. 5; Table S3).

Eighteen zircon cores from granitic gneiss DSG02 yielded Th/U ratios of 0.11–0.74 and concordant $^{207}Pb/^{206}Pb$ ages in the range of 2080 Ma to 2009 Ma with a concordia upper intercept age of 2063 ± 21 Ma (Fig. 4c), and an older weighted mean $^{207}Pb/^{206}Pb$ age of 2035 ± 7 Ma (MSWD = 1.5, n = 18) (Fig. 4d). The Th/U ratios in the metamorphic

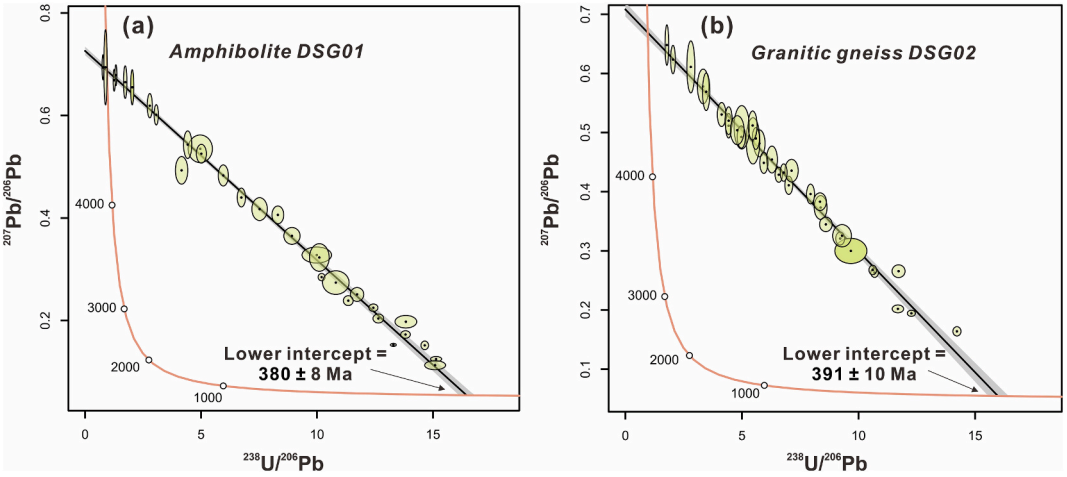


**Fig. 6.** Tera-Wasserburg concordia diagrams of U-Pb data from apatite.

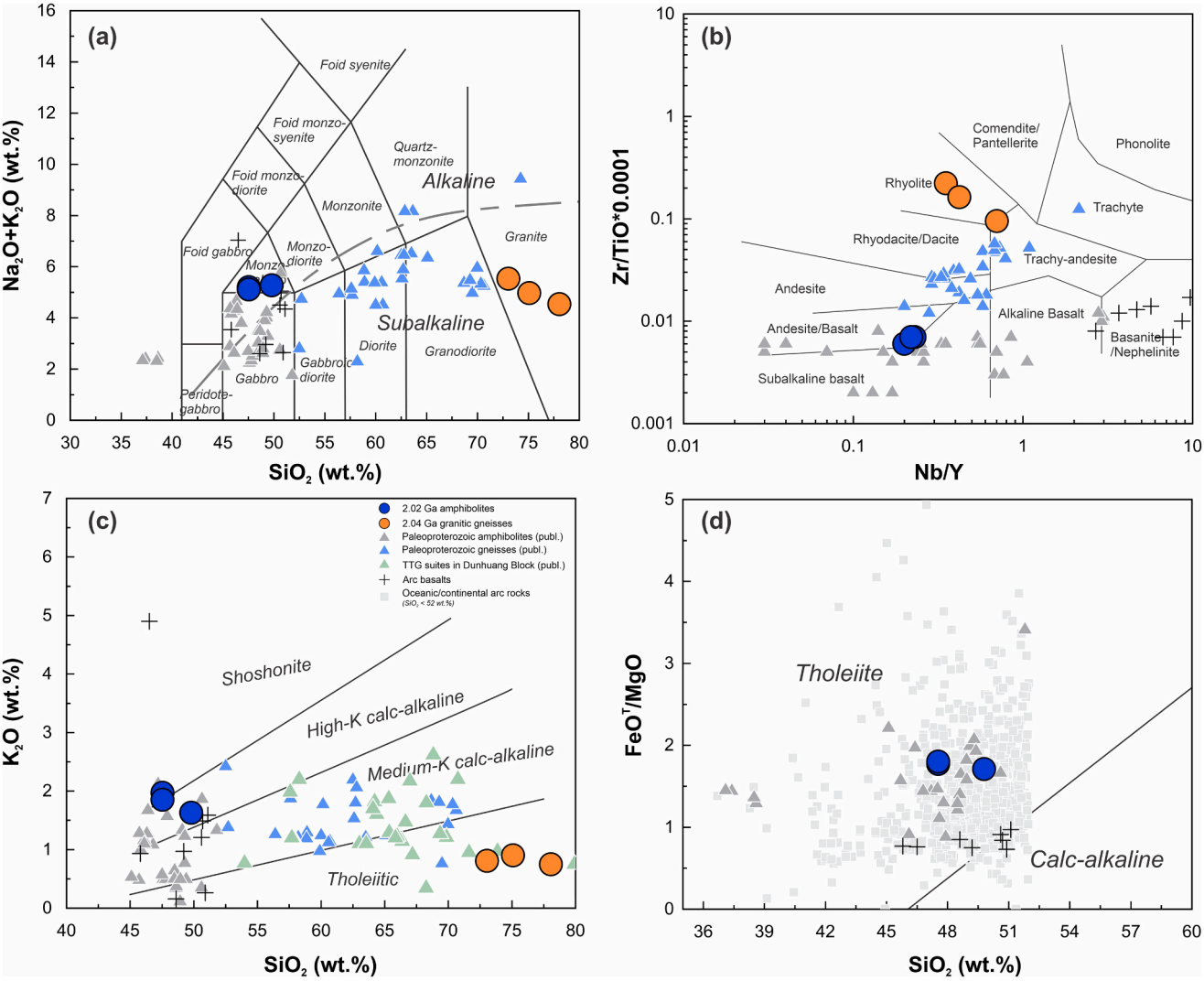


**Fig. 7.** (a) Total alkali ($Na_2O + K_2O$) versus $SiO_2$ diagram (Middlemost, 1994). (b) Zr/Ti*0.0001 versus Nb/Y (Winchester and Floyd, 1977). (c) $K_2O$ versus $SiO_2$ (Peccerillo and Taylor, 1976). (d) $FeO^T$/MgO versus $SiO_2$ (Miyashiro, 1974). Source of published geochemical data from other localities of Paleoproterozoic amphibolites and gneisses of the Dunhuang Block: He et al. (2013); Wang et al. (2013b, 2014b, 2017c, 2020), Zhu et al. (2018); Zhao et al. (2020, 2022). Data points for arc basalts in panel (a) are after Schmidt and Jagoutz (2017) and for oceanic and continental arc rocks with $SiO_2 < 52$ wt% in (d) are compiled from the GEOROC database (https://georoc.eu/georoc/).

rims are 0.19 to 0.93. The zircons yielded a concordant $^{207}Pb/^{206}Pb$ age population from 2005 to 1949 Ma with a concordia upper intercept age of 2001 ± 23 Ma (Fig. 4c). A weighted mean $^{207}Pb/^{206}Pb$ age of 1984 ± 9 Ma (MSWD = 0.59, n = 13) was calculated on thirteen ages excluding two ages with high uncertainties (Fig. 4d). The REE patterns of all analyzed zircons show positive Ce anomalies and negative Eu anomalies (Fig. S1; Table S2). Twenty-four zircons from granitic gneiss were analyzed for Lu-Hf isotopes. Eleven older zircon cores yielded $^{176}Hf/^{177}Hf$ ratios ranging from 0.281475 to 0.281598 (Table S3), $\varepsilon_{Hf}(t)$ values of −1.95 to + 1.72 (Fig. 5; Table S3), and $T_{DM2}$ values from 2767 Ma to 2544 Ma (Table S3).

### 4.2. U-Pb apatite dating

U-Pb apatite dating was performed for the same samples: amphibolite DSG01 and granitic gneiss DSG02. Apatite grains are typically oval and subhedral, columnar, 100 to 300 μm in length with aspect ratios of 1:1 to 2:1 (Fig. S2). In CL images, apatite grains from the amphibolite show typical core-rim structures and compositional zoning with bright or dark luminescence, and those from the granitic gneiss have little more complex internal structures (Fig. S2). Results of U-Pb apatite isotope analyses are presented in Table S4 and in a Tera-Wasserburg concordia diagram (Fig. 6). U-Pb apatite dating shows low Th and U abundances and Th/U ratios less than 1. All U-Pb dates of twenty-nine apatite grains from the amphibolite are discordant providing a lower intercept age of 380 ± 8 Ma (Fig. 6a). The U-Pb dates of thirty-four apatites from the granitic gneiss yielded a lower intercept age of 391 ± 10 Ma (Fig. 6b).

### 4.3. Whole-rock geochemistry

Three samples of amphibolite (DSG01-01, DSG01-02, and DSG01-03) and three samples of granitic gneiss (DSG02-01, DSG02-02, and DSG02-03) were selected for whole-rock geochemical analyses (Table S5). According to the petrographic composition and geochemical data, the samples under study are relatively fresh. Losses on ignition (LOI) ranges from 1.43 to 1.96 in the amphibolites and from 0.72 to 0.75 in the granitic gneisses.

The amphibolite samples are compositionally similar to mafic rocks with $SiO_2$ = 47.5–49.8 wt% (Fig. 7a), $Na_2O$ = 3.2–3.6 wt%, $K_2O$ = 1.6–2.0 wt%, CaO = 8.0–8.4 wt%, MgO = 5.7–6.1 wt%, and $Fe_2O_3^T$ =

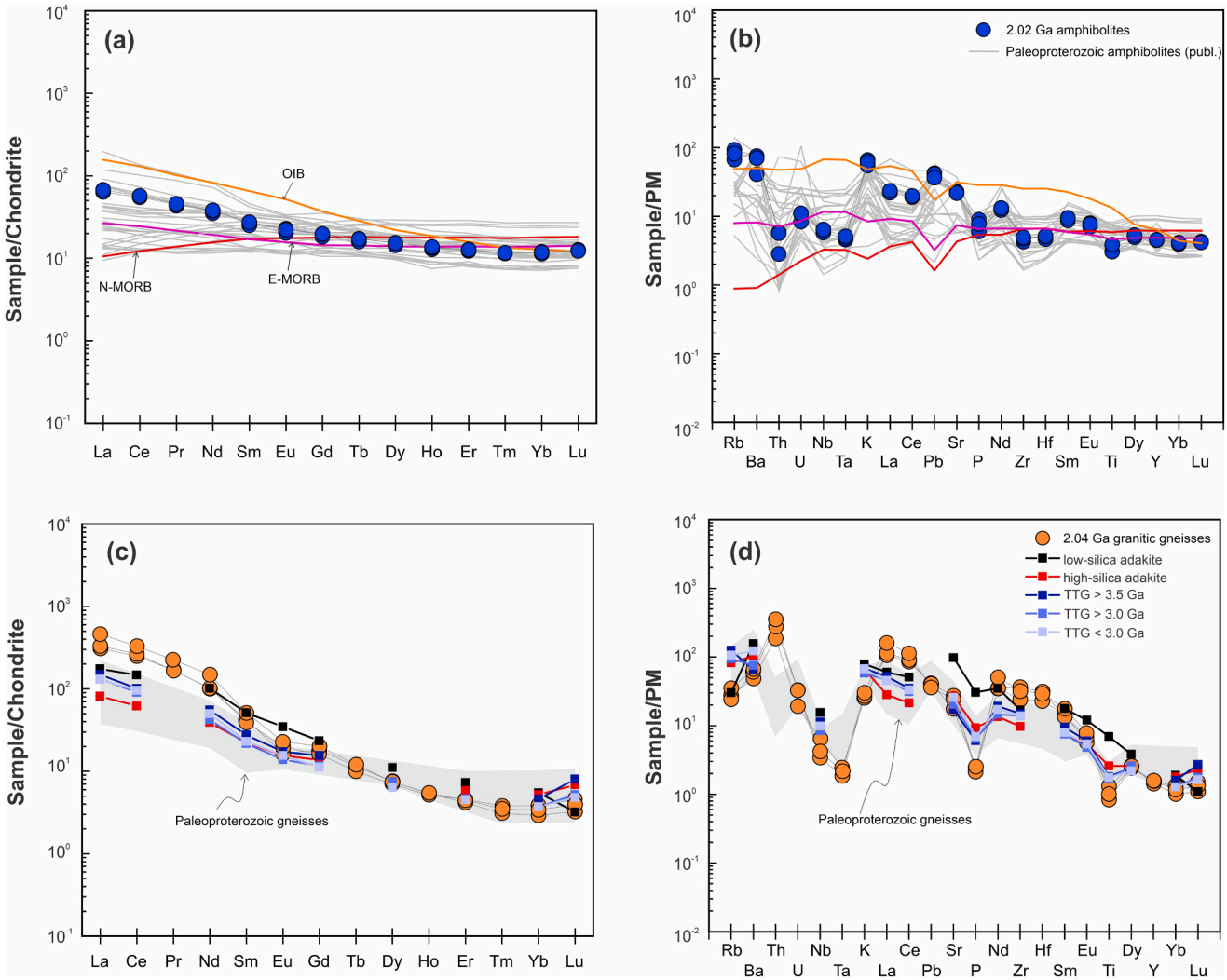


**Fig. 8.** (a, b) Chondrite-normalized rare earth element distribution patterns and (c, d) primitive mantle-normalized multi-element spidergrams for amphibolites and granitic gneisses. N-MORB, normal middle ocean ridge basalt; E-MORB, enriched middle ocean ridge basalt; OIB, oceanic island basalt; PM, primitive mantle (Sun and McDonough, 1989). Low-silica adakite, high-silica adakite and TTG represent the averages adapted from Martin et al. (2005). Data sources as in Fig. 7.

10.8–12.2 wt% (Table S5) providing moderate total alkali ($Na_2O + K_2O$ = 5.1–5.3 wt%) and Mg# of 49.7 to 51.1. Chondrite-normalized rare earth element (REE) patterns are nearly flat, with slightly enriched light REE (LREE), undifferentiated heavy REE (HREE), and no negative Eu anomalies (Eu/Eu* = 0.95–0.98). In general, such REE patterns resemble that of E-MORB, but have higher normalized LREE (Fig. 8a). In the primitive mantle normalized trace-element spidergrams, the amphibolites show peaks at Rb, Ba, K, Pb, La and Ce, and small troughs at high field strength elements (HFSEs, i.e., Zr, Hf, Nb and Ta) (Fig. 8b).

The granitic gneisses have high $SiO_2$ (73.0–78.1 wt%) and $Na_2O$ (3.79–4.72 wt%), and low CaO, MgO and $Fe_2O_3^T$ (2.80–3.21, 0.60–0.72 and 1.36–1.71 wt%, respectively; Table S5). The contents of $Al_2O_3$ are moderate (11.51–14.86 wt%), providing an aluminous saturation index (ASI = molar [$Al_2O_3$/(CaO + $K_2O$ + $Na_2O$)]) of 1.02–1.03 and accordingly they possess peraluminous features. The low contents of $K_2O$ (0.75–0.90 wt%) result in low $K_2O/Na_2O$ ratios (0.17–0.22) (Fig. 7c). In the An-Ab-Or ternary classification diagram (Fig. S3), the granitic gneisses plot in the field of trondhjemite. The REE patterns of the granitic gneisses are strongly enriched in LREE giving $(La/Yb)_N$ ratios from 87 to 136 and depleted in HREE (Fig. 8c). Unlike the amphibolites, the granitic gneisses show negative Eu anomalies (Eu/Eu* = 0.60–0.78). Their spidergrams display a higher enrichment in Th, La, Ce, Zr, and Hf, and a stronger depletion in Nb, Ta, P and Ti (Fig. 8d).

## 5. Discussion

### 5.1. Episodes of magmatism and metamorphism recorded in Paleoproterozoic meta-igneous rocks

The two types of *meta*-igneous rocks under study record episodes of both magmatism and superimposed metamorphism. The amphibolite yielded the 2021 ± 5 Ma crystallization age of its igneous protolith (Fig. 4b). The dated granitic gneiss yielded two U-Pb zircon age populations: the cores and the rims have the ages of 2035 ± 7 Ma and 1984 ± 9 Ma, respectively (Fig. 4d). The cores typically show Th/U ratios higher than 0.2, oscillatory zoning and REE distribution pattern all indicating their magmatic origin (Fig. S1). The 2.02 Ga age of zircon cores of the amphibolite match the 2.04 Ga age of zircon cores of the granitic gneiss. These Paleoproterozoic ages are consistent with the protolithic ages of other *meta*-igneous rocks of the Dunhuang Block (He et al., 2013; Zhao et al., 2015b, 2022; Zhu et al., 2018). The 1984 Ma age from CL-bright zircon rims indicates an episode of superimposed metamorphism. In addition, the U-Pb apatite age data from amphibolite and granitic gneiss define lower intercept ages of 380 ± 8 Ma (Fig. 6a) and 391 ± 10 Ma (Fig. 6b), respectively, suggesting that both Paleoproterozoic *meta*-igneous rocks under study experienced a superimposed Paleozoic tectonothermal event. The Paleozoic tectonothermal event

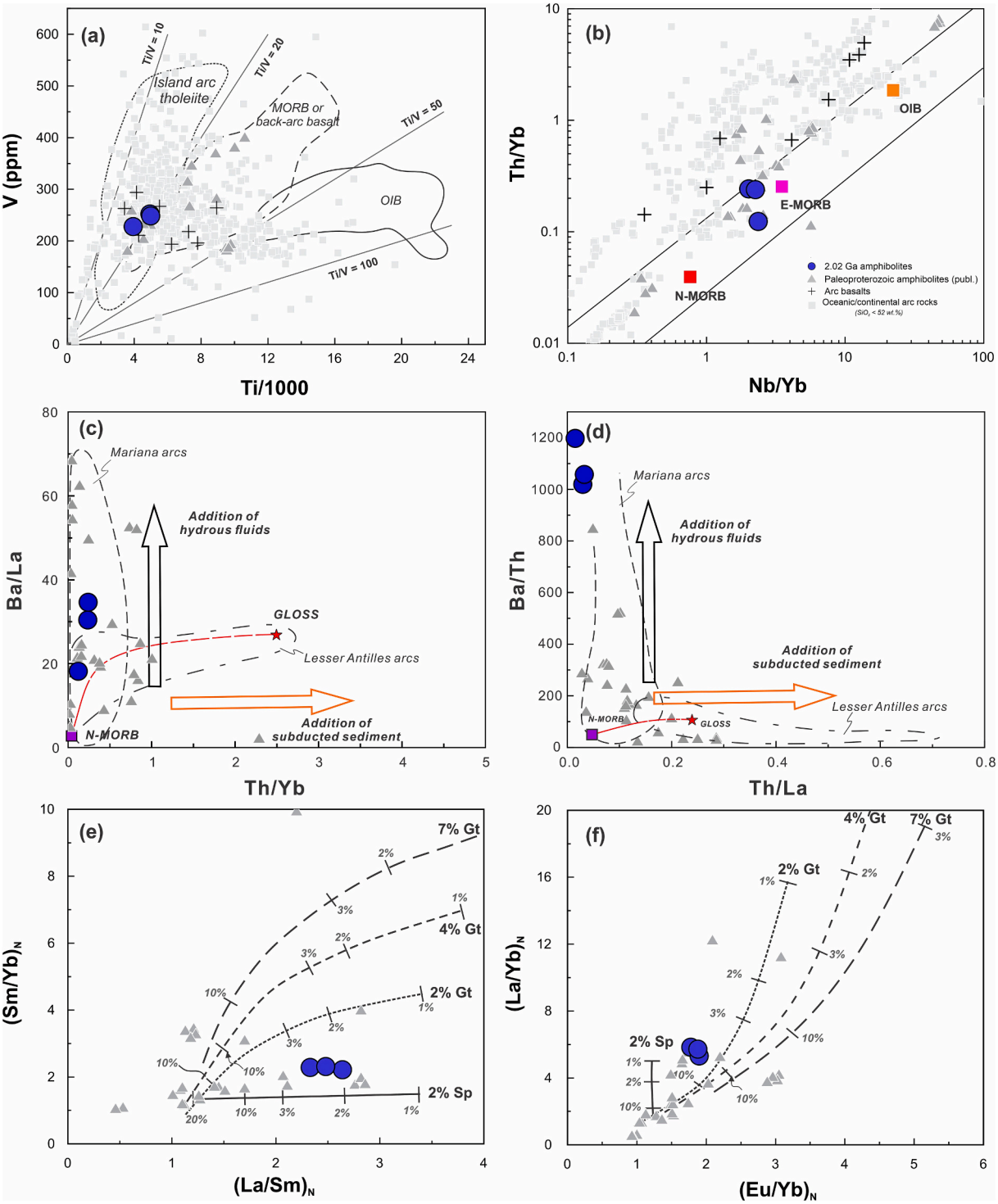


**Fig. 9.** Geochemical characteristics of Dunhuang Paleoproterozoic amphibolites. (a) V versus Ti/1000 (Shervais, 1982). (b) Th/Yb versus Nb/Yb (Pearce, 2008). (c, d) Ba/La versus Th/Yb, and Ba/Th versus Th/La diagrams illustrating contribution of slab-derived hydrous fluids and subducted sediments to the mantle sources of the magmatic protoliths of the amphibolites. Red line indicates mixing between N-MORB and global subducted sediment (GLOSS). The field outlined for the Mariana and Lesser Antilles arcs is based on the GEOROC database (https://georoc.eu/georoc/). (e, f) $(Sm/Yb)_N$ versus $(La/Sm)_N$, and $(La/Yb)_N$ versus $(Eu/Yb)_N$ diagrams in comparison with melt compositions from non-modal batch melting modeling of spinel-bearing lherzolite and garnet-bearing lherzolites (Jourdan et al., 2007). N-MORB, E-MORB and OIB are from (Sun and McDonough, 1989) and GLOSS is from (Plank and Langmuir, 1998). Data sources as in Fig. 7.

has been also documented in other localities of Precambrian rocks in Dunhuang. For example, the Neoarchean TTG rocks exposed in the Yulinhe, Gangou and Shibaocheng areas gave Paleozoic metamorphic ages of 440–390 Ma (Zong et al., 2013; Zhao et al., 2015b). The Paleoproterozoic Dongshuigou granitic gneiss (1.84 Ga), Shuwozi granitic gneiss (1.80 Ga), and the Haixia amphibolite (1.86 Ga) also yielded Paleozoic ages of superimposed metamorphism (437–367 Ma; Zhao et al., 2015b). In addition, the U-Pb apatite and titanite dating of garnet-bearing amphibolite gave younger metamorphic ages of 237 ± 4 Ma, 300 ± 10 Ma and 345 ± 3 Ma (Si et al., 2022). Therefore, we suggest

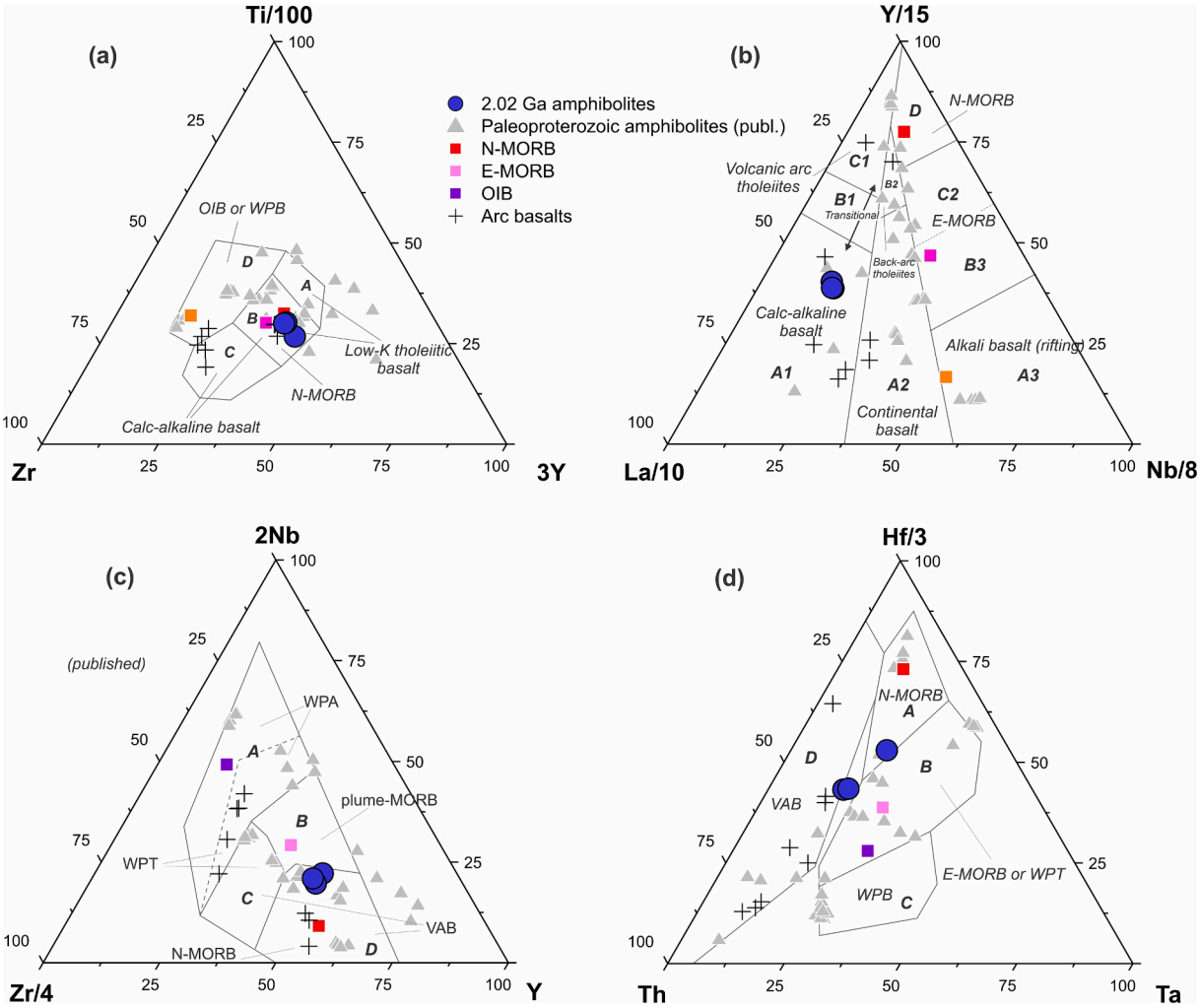


**Fig. 10.** Geochemical discrimination ternary diagrams. (a) Ti/100-Zr-3Y (after Winchester, 1984); (b) Y/15-La/10-Nb/8 (after Cabanis and Lecolle, 1989); (c) 2Nb-Zr/4-Y (after Meschede, 1986); (d) Hf/3-Th-Ta (after Wood, 1980). WPT/B, within-plate tholeiite/basalt; WPA, within-plate alkali basalt; VAB, volcanic arc basalt. Data sources as in Fig. 7.

that in Paleozoic time those Precambrian rocks of the Dunhuang Block commonly experienced superimposed metamorphism. Evidence for active Paleozoic tectonothermal events in the Dunhuang Block comes from many other localities of magmatic and metamorphic complexes (Zong et al., 2012; Wang et al., 2016, 2017a, 2017b, 2018; Zhao et al., 2016; Gan et al., 2024).

### 5.2. *Petrogenesis of Paleoproterozoic meta-igneous rocks*

Although the rocks under study are metamorphic, amphibolites and granitic gneisses, they are *ortho*-metamorphic rocks or *meta*-igneous rocks, i.e. formed by metamorphism of igneous rocks. The geochemical and petrographic data suggest that magmatic protoliths of the metamorphic rocks probably experienced low-degree to nil post-magmatic alteration. There are few if any typical secondary minerals (chlorite, epidote, calcite; Fig. 3d, e) and the rocks gave relatively low LOI (0.72–1.96; Table S5).

#### 5.2.1. *Amphibolites*

In section 4, we argue that the protoliths of the amphibolites were igneous rocks (Figs. 1a, c, 4a). In the $TiO_2$ versus MnO and Ni versus Zr/$TiO_2$ diagrams, the amphibolites are plotted in the *ortho*-amphibolite field (Fig. S4). The Mg# values (49.7–50.2) and the concentrations of Cr (85–95 ppm) and Ni (28–38 ppm) are all notably lower than those in primitive magmas (Mg# > 64; Cr > 400 ppm, Ni > 200 ppm; Tatsumi and Eggins, 1995). Therefore, the protoliths of the amphibolites were evolved magmas, which petrogenesis could be affected by crustal contamination or fractional crystallization. In term of crustal contamination, the amphibolites have less variable compositions of both major oxides and trace elements compared to typical crustal materials that have higher concentrations of Th (5.6 ppm in average), higher Th/Nb (0.7 in average) and La/Sm (5.13 in average) compared to depleted MORB (Rudnick and Gao, 2003). However, the Dunhuang amphibolites have lower Th (0.24–0.49), Th/Nb (0.05–0.12) and La/Sm (3.60–4.09). Accordingly, we suggest that crustal contamination played an insignificant role in the evolution of the protolithic magmas. In term of fractional crystallization, the contents of Ni, Cr, and Co gradually decrease as MgO decreases that can be explained by fractionation of olivine and pyroxene (Sato, 1977; Nabelek, 1980; Barnes, 1986; Roux et al., 2011). The Eu negative anomalies are very small (Eu/Eu* = 0.95–0.98) suggesting minor fractionation of plagioclase (Fig. 8a). The troughs at Ti in the spidergrams (Fig. 8b) suggest fractionation of Fe-Ti oxides. Therefore, the parental magmas of the igneous protoliths of the amphibolites probably underwent fractionation of olivine, pyroxene and Fe-Ti oxides.

The protoliths of the amphibolites could be subalkaline basaltic magmas as seen in the $SiO_2$ versus $K_2O$ diagram (Fig. 7c), but their $SiO_2$ versus $FeO^T$/MgO diagram (Fig. 7d) and the Ti versus V systematics (Fig. 9a) show a tholeiitic affinity. Although the amphibolites are plotted

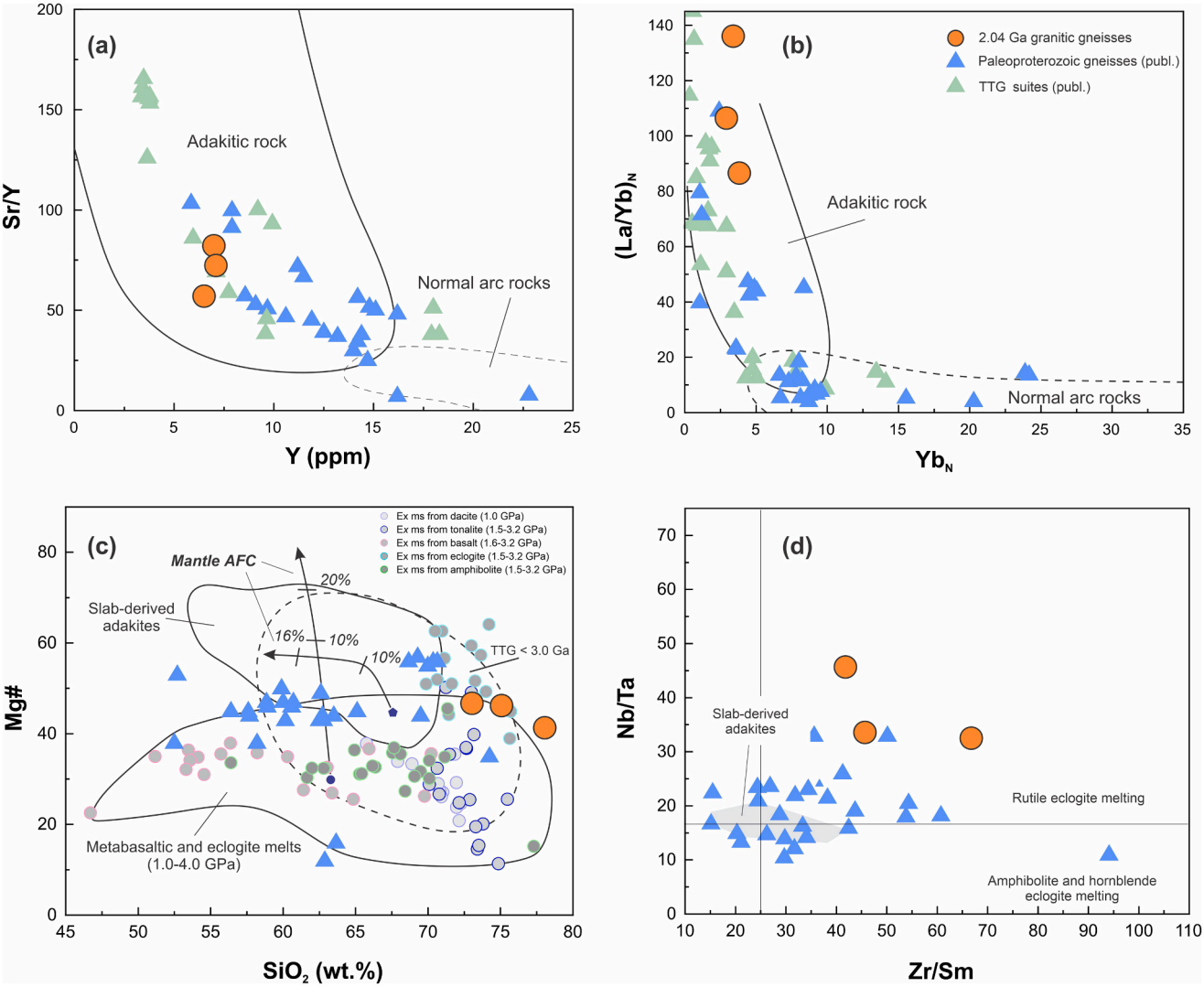


**Fig. 11.** Geochemical characteristics of the Paleoproterozoic granitic gneisses. (a) Sr/Y versus Y (Drummond and Defant, 1990); (b) $(La/Yb)_N$ versus $Yb_N$ (Martin, 1986); (c) Mg# versus $SiO_2$: the field of slab-derived adakites, metabasaltic and eclogite melts derived at 1.0–4.0 Ga are after (Wang et al., 2007); the field of < 3.0 Ga TTG is after (Smithies, 2000); mantle AFC (assimilation and fractional crystallization) curves are adapted from (Stern and Kilian, 1996; Rapp et al., 1999); sources for experimental melts (abbreviated as Ex ms) for different start compositions are (Rapp et al., 1991; Sen and Dunn, 1994; Rapp and Watson, 1995; Skjerlie and Patiño-Douce, 2002; Patiño Douce, 2005). (d) Nb/Ta versus Zr/Sm (Condie, 2005), and the melting fields are from (Foley et al., 2002). Data points of Paleoproterozoic gneisses are as in Fig. 7.

within the N-MORB and OIB mantle array and near E-MORB in the Th/Yb versus Nb/Yb diagram (Fig. 9b), their REE patterns and spidergrams are different from that of E-MORB as they are characterized by enriched LREE and LILEs (e.g., Rb, Ba and Sr) and troughs at Nb-Ta (Fig. 8a, b).

The mantle sources of the protoliths were possibly affected by crustal material because they show enrichment in incompatible elements (e.g., Rb, Ba, K and LREEs; Fig. 8a, b). The amphibolites have depleted Hf-in-zircon isotope compositions with low to moderate $\varepsilon_{Hf}(t)$ values of + 0.71 to + 4.93 (Fig. 5), indicating that the amphibolites were produced by melting of a slightly enriched mantle source. Crustal contamination is usually considered to be a key magmatic process to contribute to evolved compositions of mantle-derived magmas (Wooden et al., 1993; Haase et al., 2004; Mungall, 2007). However, as we discussed above, crustal contamination hardly had a notable impact on the variation of trace elements in the amphibolites. A mantle wedge source may be enriched in Ba, Rb, Th, U, K and LREEs and depleted in Nb-Ta during interaction with melts or fluids released from the subducting slab (e.g., Tatsumi et al., 1986; Hawkesworth et al., 1993; Elliott et al., 1997; Grove et al., 2002; Plank, 2005; Spandler and Pirard, 2013).

Elemental LILE/HFSE ratios, such as La/Nb can be used to trace the enrichment of mantle sources by subducted materials (Rudnick, 1995; Condie, 1999, 2003a; Hanyu et al., 2006). The higher La/Nb ratios (3.44–3.66) relative to N-MORB (La/Nb = 1.07; Sun and McDonough, 1989) suggest that the amphibolites were probably derived from a mantle wedge that was enriched by subducted materials prior to the melting. The very high ratio of Ba/Th (1019–1197) and Ba/La (18–35), but low Th/La (0.015–0.033) and Th/Yb (0.12–0.24) suggest rather metasomatism of the mantle source by slab-derived fluids than participation of melted subducted sediments like in the case of the Mariana intra-oceanic arc (Fig. 9c, d; Woodhead et al., 2001; Plank, 2005; Hanyu et al., 2006). The Ce/Pb ratios (4.36–5.20) are lower than that of N-MORB (Ce/Pb > 20; Sun and McDonough, 1989) and also support the contribution of slab fluids based on the principle of preferential partitioning of Pb with respect to Ce (Brenan et al., 1995; Kogiso et al., 1997). To evaluate the degree of the melting, we compared chondrite-normalized REE ratios of the amphibolites with those of modeled melts derived by a non-modal equilibrium melting of garnet-bearing and spinel-bearing lherzolites (Jourdan et al., 2007). The results show that

**Table 1**
A summary of Neoarchean-Paleoproterozoic magmatic and metamorphic rocks in the Dunhuang Block.

| Sample no. | Lithology | Location | Age (Ma) | Age type | References |
|---|---|---|---|---|---|
| XLP-1 | Tonalitic gneiss | Aktashtagh | 2532 | Magmatic | Long et al. 2014 |
| XLP-16 | Tonalitic gneiss | Aktashtagh | 2727 | Magmatic | Long et al. 2014 |
| XLP-30 | Monzogranitic gneiss | Aktashtagh | 2511 | Magmatic | Long et al. 2014 |
| XILP01 | Metadiorite | Aktashtagh | 2498 | Magmatic | Long et al. 2014 |
| Wl18-8–3.5 | Granitic dyke | Aktashtagh | 1847 | Magmatic | Lv et al. 2020 |
| AKS09 | Meta-felsic rock | Aktashtagh | 1963 | Magmatic | Wang et al., 2017c |
| AKS12 | Meta-mafic rock | Aktashtagh | 2061 | Magmatic | Wang et al., 2017c |
| AK07 | Amphibole plagiogneiss | Aktashtagh | 2545 | Magmatic | Wang et al. 2020 |
| AK17 | Biotite plagiogneiss | Aktashtagh | 2514 | Magmatic | Wang et al. 2020 |
| AK05 | Amphibolite | Aktashtagh | 1964 | Metamorphic | Wang et al. 2020 |
| AK07 | Amphibole plagiogneiss | Aktashtagh | 2065 | Metamorphic | Wang et al. 2020 |
| AK28 | Garnet-biotite gneiss | Aktashtagh | 2028 | Magmatic | Wang et al. 2020 |
| AK5 | Amphibolite | Aktashtagh | 1961 | Metamorphic | Zhang et al. 2019 |
| AK21 | Garnet biotite gneiss | Aktashtagh | 1845 | Metamorphic | Zhang et al. 2019 |
| AK3 | Garnet biotite gneiss | Aktashtagh | 1972 | Metamorphic | Zhang et al. 2019 |
| Y027 | Quartz monzonitic dyke | Aktashtagh | 1825 | Magmatic | Lu and Yuan 2003 |
| Y023 | Trondhjemitic gneiss | Aktashtagh | 2374 | Magmatic | Lu and Yuan 2003 |
| Y026 | Tonalitic gneiss | Aktashtagh | 2604 | Magmatic | Lu and Yuan 2003 |
| Y025 | Monzogranitic gneiss | Aktashtagh | 2830 | Magmatic | Lu et al. 2008 |
| I9809 | Granitic gneiss | Aktashtagh | 3665 | Magmatic | Lu et al. 2008 |
| I9809 | Granitic gneiss | Aktashtagh | 2396 | Magmatic | Lu et al. 2008 |
| 15ALT10 | Tonalitic gneiss | Aktashtagh | 3704 | Magmatic | Ge et al., 2018 |
| 15ALT10 | Tonalitic gneiss | Aktashtagh | 3570 | Metamorphic | Ge et al., 2018 |
| 15ALT10 | Tonalitic gneiss | Aktashtagh | 2000 | Metamorphic | Ge et al., 2018 |
| 16ALT01 | Tonalitic gneiss | Aktashtagh | 3717 | Magmatic | Ge et al., 2018 |
| 16ALT04 | Tonalitic gneiss | Aktashtagh | 3549 | Metamorphic | Ge et al., 2018 |
| 16ALT04 | Tonalitic gneiss | Aktashtagh | 1971 | Metamorphic | Ge et al., 2018 |
| 16ALT05 | Tonalitic gneiss | Aktashtagh | 3686 | Magmatic | Ge et al., 2018 |
| 16ALT08 | Tonalitic gneiss | Aktashtagh | 3719 | Magmatic | Ge et al., 2018 |
| 16ALT09 | Tonalitic gneiss | Aktashtagh | 2041 | Magmatic | Zhu et al. 2018 |
| 16ALT10 | Dioritic gneiss | Aktashtagh | 2031 | Magmatic | Zhu et al. 2018 |
| 15ALT07 | Amphibolite | Aktashtagh | 2012 | Metamorphic | Zhu et al. 2018 |
| 15ALT12 | Cpx-bearing amphibolite | Aktashtagh | 2048 | Metamorphic | Zhu et al. 2018 |
| SKZ06 | Granodioritic gneiss | Shangkouzigou | 2003 | Magmatic | Yan 2017 |
| SKZ09 | Biotite amphibole plagiogneiss | Shangkouzigou | 1991 | Magmatic | Yan 2017 |
| YHX02 | Trondhjemitic gneiss | Yinghuxia | 2557 | Magmatic | Yan et al., 2024 |
| YHX02 | Trondhjemitic gneiss | Yinghuxia | 2051 | Metamorphic | Yan et al., 2024 |
| SKZ06 | Granodioritic gneiss | Shangkouzigou | 1814 | Metamorphic | Yan 2017 |
| SKZ08 | Trondhjemitic gneiss | Shangkouzigou | 2618 | Magmatic | Yan et al., 2024 |
| SKZ08 | Trondhjemitic gneiss | Shangkouzigou | 2455 | Metamorphic | Yan et al., 2024 |
| SKZ08 | Trondhjemitic gneiss | Shangkouzigou | 2040 | Metamorphic | Yan et al., 2024 |
| SKZ07 | Trondhjemitic gneiss | Shangkouzigou | 2547 | Magmatic | Yan et al., 2024 |
| SKZ07 | Trondhjemitic gneiss | Shangkouzigou | 2467 | Metamorphic | Yan et al., 2024 |
| AQ11-13–1.1 | A-type granite | Sanweishan | 1776 | Magmatic | Yu et al. 2014 |
| AQ11-13–1.3 | A-type granite | Sanweishan | 1777 | Magmatic | Yu et al. 2014 |
| AQ11-13–1.4 | A-type granite | Sanweishan | 1759 | Magmatic | Yu et al. 2014 |
| HYS01 | A-type granite | Huoyanshan | 1791 | Magmatic | Gan et al. 2020 |
| HYS02 | A-type granite | Huoyanshan | 1787 | Magmatic | Gan et al. 2020 |
| HYS08 | A-type granite | Huoyanshan | 1786 | Magmatic | Gan et al. 2020 |
| X10-4–1 | Amphibolite | Sanweishan | 1987 | Magmatic | He et al. 2013 |
| X10-9–1 | Augen gneiss | Danghe reservoir | 1852 | Magmatic | He et al. 2013 |
| X10-5–2 | Augen gneiss | Sanweishan | 1733 | Magmatic | He et al. 2013 |
| X10-1–8 | Augen gneiss | Sanweishan | 1767 | Magmatic | He et al. 2013 |
| Wl18-9–3.1 | Granite | Huoyanshan | 1757 | Magmatic | Lv et al. 2020 |
| Wl18-9–1.1 | Mafic granulite | Shibaocheng | 1815 | Metamorphic | Lv et al. 2020 |
| 19SBC01 | Garnet amphibolite | Shibaocheng | 1830 | Metamorphic | Si et al. 2022 |
| 19SBC02 | Garnet amphibolite | Shibaocheng | 1822 | Metamorphic | Si et al. 2022 |
| 20SBC03 | Garnet amphibolite | Shibaocheng | 1846 | Metamorphic | Si et al. 2022 |
| 20GG09 | Garnet amphibolite | Gangou | 1951 | Metamorphic | Si et al. 2022 |
| HLX05 | Quartz–micaschist | Hongliuxia | 1818 | Metamorphic | Wang et al. 2013a |
| HLX17-2 | Garnet-bearing biotite–plagioclase gneiss | Hongliuxia | 1830 | Metamorphic | Wang et al. 2013a |
| HLX29 | Kyanite-bearing biotite–plagioclase gneiss | Hongliuxia | 1833 | Metamorphic | Wang et al. 2013a |
| HLX19-2 | Garnet-bearing amphibolite | Hongliuxia | 1830 | Magmatic | Wang et al., 2014b |
| HLX08-1 | Garnet-bearing amphibolite | Hongliuxia | 1608 | Magmatic | Wang et al., 2014b |
| YLH01 | Tonalite | Yulin river | 2485 | Magmatic | Zhao et al. 2015b |
| YLH03 | Tonalite | Yulin river | 2452 | Magmatic | Zhao et al. 2015b |
| YLH06 | Tonalite | Yulinhe reservoir | 2004 | Magmatic | Zhao et al. 2015b |
| GG09 | Granodiorite | Gangou | 2630 | Magmatic | Zhao et al. 2015b |
| GG10 | Tonalite | Gangou | 2635 | Magmatic | Zhao et al. 2015b |
| SBC09 | Tonalite | Shibaocheng | 2556 | Magmatic | Zhao et al. 2015b |
| YLH01 | Tonalite | Yulin river | 1878 | Metamorphic | Zhao et al. 2015b |
| YLH03 | Tonalite | Yulin river | 1825 | Metamorphic | Zhao et al. 2015b |
| GG09 | Granodiorite | Gangou | 1936 | Metamorphic | Zhao et al. 2015b |
| GG10 | Tonalite | Gangou | 2031 | Metamorphic | Zhao et al. 2015b |

(*continued on next page*)

**Table 1** (*continued*)

| Sample no. | Lithology | Location | Age (Ma) | Age type | References |
|---|---|---|---|---|---|
| 1311GG11 | Granodioritic gneiss | Gangou | 3056 | Magmatic | Zhao et al. 2015a |
| 1311GG11 | Granodioritic gneiss | Gangou | 1922 | Metamorphic | Zhao et al. 2015a |
| X11-113–2 | Trondhjemitic gneiss | Langchaigou | 2717 | Magmatic | Zong et al. 2013 |
| X11-114–1 | Trondhjemitic gneiss | Langchaigou | 2642 | Magmatic | Zong et al. 2013 |
| X11-122–1 | Trondhjemitic gneiss | Langchaigou | 2708 | Magmatic | Zong et al. 2013 |
| X11-113–2 | Trondhjemitic gneiss | Langchaigou | 1914 | Metamorphic | Zong et al. 2013 |
| X11-114–1 | Trondhjemitic gneiss | Langchaigou | 2002 | Metamorphic | Zong et al. 2013 |
| X11-122–1 | Trondhjemitic gneiss | Langchaigou | 1966 | Metamorphic | Zong et al. 2013 |
| AQ10-4–4.1 | HP mafic granulite | Shibaocheng | 1842 | Metamorphic | Zhang et al., 2012b |
| AQ10-4–2.3 | HP mafic granulite | Shibaocheng | 1834 | Metamorphic | Zhang et al., 2012b |
| AQ10-4–1.1 | Tonalitic gneiss | Shibaocheng | 2549 | Magmatic | Zhang et al. 2013b |
| AQ10-4–2.2 | Tonalitic gneiss | Shibaocheng | 2489 | Magmatic | Zhang et al. 2013b |
| AQ10-11–4.1 | Granodioritic gneiss | Hongliuxia | 2533 | Magmatic | Zhang et al. 2013b |
| T08-12–3.3 | Granodioritic gneiss | Hongliuxia | 2299 | Magmatic | Zhang et al. 2013b |
| T08-12–1.1 | Granodioritic gneiss | Hongliuxia | 2332 | Magmatic | Zhang et al. 2013b |
| AQ10-4–4.1 | HP mafic granulite | Shibaocheng | 1818 | Metamorphic | Zhang et al. 2013b |
| AQ10-4–1.1 | Tonalitic gneiss | Shibaocheng | 1885 | Metamorphic | Zhang et al. 2013b |
| AQ10-12–2.1 | Tonalitic gneiss | Haobula | 1829 | Metamorphic | Zhang et al. 2013b |
| AQ10-11–4.1 | Granodioritic gneiss | Hongliuxia | 1825 | Metamorphic | Zhang et al. 2013b |
| T08-12–3.3 | Granodioritic gneiss | Hongliuxia | 1828 | Metamorphic | Zhang et al. 2013b |
| T08-12–1.1 | Granodioritic gneiss | Hongliuxia | 1842 | Metamorphic | Zhang et al. 2013b |
| SXK29 | Amphibolite | Shuixiakou | 1807 | Metamorphic | Zhao et al. 2013 |
| SXK-31 | Tonalitic gneiss | Shuixiakou | 2561 | Magmatic | Zhao et al. 2013 |
| SXK-30 | Granitic gneiss | Shuixiakou | 2510 | Magmatic | Zhao et al. 2013 |
| 1318HLX18 | Dioritic gneiss | Hongliuxia | 2045 | Magmatic | Zhao et al. 2022 |
| 1405GG04 | Granodioritic gneiss | Gangou | 1998 | Magmatic | Zhao et al. 2022 |
| 1312GG12 | Potassic granite | Gangou | 1950 | Magmatic | Zhao et al. 2022 |
| 17DBT10 | Granodioritic gneiss | Gangou | 2057 | Magmatic | Diao 2018 |
| 17DBT16 | Granitic gneiss | Dashuixia | 1842 | Magmatic | Diao 2018 |
| 17SWS09 | Granodioritic gneiss | Dongshuigou | 1846 | Magmatic | Diao 2018 |
| 17HLX03 | Granodioritic gneiss | Hongliuxia | 2376 | Magmatic | Diao 2018 |
| 17DBT10 | Granodioritic gneiss | Gangou | 1884 | Metamorphic | Diao 2018 |
| 17HLX03 | Granodioritic gneiss | Hongliuxia | 1888 | Metamorphic | Diao 2018 |
| 1302SWS02 | Rhyolite | Sanweishan | 1838 | Magmatic | Zhao et al. 2020 |
| 1307DSG07 | Granite | Dongshuigou | 1839 | Magmatic | Zhao et al. 2020 |
| 1308DSG08 | Granite | Dongshuigou | 1820 | Magmatic | Zhao et al. 2020 |
| 1310SWZ10 | Granitic gneiss | Shuwozi | 1805 | Magmatic | Zhao et al. 2020 |
| 1306HX06 | Amphibolite | Hanxia | 1861 | Magmatic | Zhao et al. 2020 |
| 19DH-1 | Metapelite | Mogutai | 1812 | Metamorphic | Zhao et al. 2020 |
| 13SWS | Muscovite-quartz schist | Sanweishan | 1818 | Metamorphic | Zhao et al., 2019b |
| 09HX | Biotite-quartz schist | Hanxia | 1802 | Metamorphic | Zhao et al., 2019b |
| 1432MGT01 | Garnel-sillimanite-bearing mica-quartz schist | Mogutai | 1813 | Metamorphic | Zhao et al., 2019b |
| 1433MGT02 | Garnet-bearing mica-quartz schist | Mogutai | 1818 | Metamorphic | Zhao et al., 2019b |
| 1324HLX24 | Quartzite | Hongliuxia | 1810 | Metamorphic | Zhao et al., 2019b |
| 1304YLH04 | Amphibolite | Yulinhe | 1876 | Magmatic | Zhao 2017 |
| HYS09 | Potassic granite | Huoyanshan | 1786 | Magmatic | Zhao et al., 2019a |
| HLX26 | Amphibolite | Hongliuxia | 1605 | Magmatic | Zhao et al., 2019a |
| HLX08 | Amphibolite | Hongliuxia | 1611 | Magmatic | Wang et al. 2013b |
| 1312GG12 | Potassic granite | Gangou | 1950 | Magmatic | Zhao et al. 2022 |
| 17DBT10 | Granodioritic gneiss | Gangou | 2057 | Magmatic | Diao 2018 |
| 17DBT16 | Granitic gneiss | Dashuixia | 1842 | Magmatic | Diao 2018 |
| 17SWS09 | Granodioritic gneiss | Dongshuigou | 1846 | Magmatic | Diao 2018 |
| 17HLX03 | Granodioritic gneiss | Hongliuxia | 2376 | Magmatic | Diao 2018 |
| 17DBT10 | Granodioritic gneiss | Gangou | 1884 | Metamorphic | Diao 2018 |
| 17HLX03 | Granodioritic gneiss | Hongliuxia | 1888 | Metamorphic | Diao 2018 |
| 1302SWS02 | Rhyolite | Sanweishan | 1838 | Magmatic | Zhao et al. 2020 |
| 1307DSG07 | Granite | Dongshuigou | 1839 | Magmatic | Zhao et al. 2020 |
| 1308DSG08 | Granite | Dongshuigou | 1820 | Magmatic | Zhao et al. 2020 |
| 1310SWZ10 | Granitic gneiss | Shuwozi | 1805 | Magmatic | Zhao et al. 2020 |
| 1306HX06 | Amphibolite | Hanxia | 1861 | Magmatic | Zhao et al. 2020 |
| 19DH-1 | Metapelite | Mogutai | 1812 | Metamorphic | Zhao et al. 2020 |
| 13SWS | Muscovite-quartz schist | Sanweishan | 1818 | Metamorphic | Zhao et al., 2019b |
| 09HX | Biotite-quartz schist | Hanxia | 1802 | Metamorphic | Zhao et al., 2019b |
| 1432MGT01 | Garnel-sillimanite-bearing mica-quartz schist | Mogutai | 1813 | Metamorphic | Zhao et al., 2019b |
| 1433MGT02 | Garnet-bearing mica-quartz schist | Mogutai | 1818 | Metamorphic | Zhao et al., 2019b |
| 1324HLX24 | Quartzite | Hongliuxia | 1810 | Metamorphic | Zhao et al., 2019b |
| 1304YLH04 | Amphibolite | Yulinhe | 1876 | Magmatic | Zhao 2017 |
| HYS09 | Potassic granite | Huoyanshan | 1786 | Magmatic | Zhao et al., 2019a |
| HLX26 | Amphibolite | Hongliuxia | 1605 | Magmatic | Zhao et al., 2019a |
| HLX08 | Amphibolite | Hongliuxia | 1611 | Magmatic | Wang et al. 2013b |
| 1306HX06 | Amphibolite | Hanxia | 1861 | Magmatic | Zhao et al. 2020 |
| 19DH-1 | Metapelite | Mogutai | 1812 | Metamorphic | Zhao et al. 2020 |
| 13SWS | Muscovite-quartz schist | Sanweishan | 1818 | Metamorphic | Zhao et al., 2019b |
| 09HX | Biotite-quartz schist | Hanxia | 1802 | Metamorphic | Zhao et al., 2019b |
| 1432MGT01 | Garnel-sillimanite-bearing mica-quartz schist | Mogutai | 1813 | Metamorphic | Zhao et al., 2019b |
| 1433MGT02 | Garnet-bearing mica-quartz schist | Mogutai | 1818 | Metamorphic | Zhao et al., 2019b |

(*continued on next page*)

**Table 1** (*continued*)

| Sample no. | Lithology | Location | Age (Ma) | Age type | References |
|---|---|---|---|---|---|
| 1324HLX24 | Quartzite | Hongliuxia | 1810 | Metamorphic | Zhao et al., 2019b |
| 1304YLH04 | Amphibolite | Yulinhe | 1876 | Magmatic | Zhao 2017 |
| HYS09 | Potassic granite | Huoyanshan | 1786 | Magmatic | Zhao et al., 2019a |
| HLX26 | Amphibolite | Hongliuxia | 1605 | Magmatic | Zhao et al., 2019a |
| HLX08 | Amphibolite | Hongliuxia | 1611 | Magmatic | Wang et al. 2013b |
| DSG01 | Amphibolite | Dongshuigou | 2021 | Magmatic | ***this study*** |
| DSG02 | Granitic gneiss | Dongshuigou | 2035 | Magmatic | ***this study*** |
| DSG02 | Granitic gneiss | Dongshuigou | 1984 | Metamorphic | ***this study*** |

amphibolites plot between the melting curves of garnet lherzolites and spinel lherzolite at a low degree (Fig. 9e, f). In the Ti-Zr-Y, Y-La-Nb, Nb-Zr-Y and Hf-Th-Ta tectonic discrimination diagrams (Fig. 10a-d), the amphibolites plot in the fields of volcanic arcs. Therefore, we conclude that the igneous protoliths of the amphibolites were derived by a low degree of melting of a mantle wedge that was metasomatized by subduction related fluids in a supra-subduction tectonic setting.

#### 5.2.2. *Granitic gneisses*

The granitic gneisses have high $SiO_2$ (73.0–78.1 wt%) and $Na_2O$ (3.8–4.7 wt%), but low $K_2O/Na_2O$ ratios (0.17–0.22 wt%). They are enriched in LREE and depleted in HREE (Fig. 8c) and show high ratios of Sr/Y (57–82) and $(La/Yb)_N$ (86–136) (Fig. 11a, b). Therefore, the granitic gneisses possess geochemical affinities to TTG or high-silica adakitic rocks (Martin, 1999; Martin et al., 2005). As far as the granitic gneisses are high-silica rocks ($SiO_2 > 72$ wt%), they cannot be correlated even with high-silica adakites which mostly have a content of $SiO_2$ lower than 60 wt% (Martin et al., 2005). In addition, the extent of LREE enrichment ($(La/Yb)_N = 87–136$) is higher and the concentrations of MgO, Cr and Ni are lower than those in typical high-silica adakites (Fig. 8c) (Martin et al., 2005; Rapp et al., 1999, 2003, 2010). Finally, the granitic gneisses are characterized by the values of Nb/Ta (33–46) and Zr/Sm (42–67) higher than those of slab-derived adakites (Fig. 11d). All these features rule out an adakite-type nature of the granitic gneisses.

Alternatively, the compositions of the granitic gneisses can be compared with TTG. In the Or-An-Ab diagram, the granitic gneisses plot at the boundary between the fields of trondhjemite and tonalite, i.e., match the TTG composition (Fig. S3). In general, a typical scenario for the petrogenesis of TTG implies hydrous melting of eclogite or enriched basaltic rocks at island arc/oceanic plateau (Smithies, 2000; Rapp et al., 2003; Smithies et al., 2009; Moyen and Martin, 2012; Palin et al., 2016). However, the available experimental data suggested that the high-pressure low-degree melting of mafic rocks tend to produce silica-rich trondhjemitic or tonalitic rocks ($SiO_2 > 70$ wt%) (Fig. 11c; Rapp and Watson, 1995; Skjerlie and Patiño-Douce, 2002).

In the Dunhuang Group, the granitic gneisses are exposed as large bodies rather than thin felsic veins (Fig. 3a) excluding the low-degree melting scenario. In addition, the Dunhuang granitic gneisses display more evolved Hf-in-zircon isotopic compositions ($\varepsilon_{Hf}(t) = -1.95$ to $+1.72$) than the coeval mafic rocks with more positive $\varepsilon_{Hf}(t)$ values reaching $+4.93$ (Fig. 5). Such a difference in isotope characteristics also argues against the origin of the granitic gneisses by melting of mafic rocks. In the age versus $\varepsilon_{Hf}(t)$ diagram, the cores of zircons from the granitic gneiss and the 2.6–2.5 Ga zircon from other TTG rocks of the Dunhuang Block plot between 3.0 Ga and 2.5 Ga crustal evolutionary arrays and show relatively enriched $\varepsilon_{Hf}(t)$ values ranging from $-1.95$ to $+1.72$ (Fig. 5). Thus, our data suggest that the granitic gneisses were probably derived by re-melting of the ca. 2.6–2.5 Ga TTG rocks due to heat input of mantle-derived magmas as coeval mafic rocks are spatially related to the granitic gneisses. The emplacement of the granitic gneisses may represent an episode of crustal anatexis event at ~ 2.04 Ga within the Dunhuang Block.

### 5.3. *Tectonic evolution of the Dunhuang Block in the Neoarchean-Paleoproterozoic*

The Dunhuang Block is dominated by Neoarchean TTG rocks and Paleoproterozoic gneissic rocks implying the presence of an ancient continental nucleus (Lu et al., 2008; Zong et al., 2013; Zhao et al., 2015b). Previously, the Dunhuang Block has been considered as a part of the TC (Long et al., 2014; Zhao et al., 2015b; Wan et al., 2018), or it has been correlated with the Alxa Block that is located in the western NCC during the Neoarchean-Paleoproterozoic (Zhang et al., 2012b, 2013b; He et al., 2013). An alternative suggestion is that from the Neoarchean to the early Paleoproterozoic the Tarim, Dunhuang and Alxa blocks probably composed a single continental landmass (Chen et al., 2013; Ge et al., 2013b, 2015).

A large number of robust geochronological data from magmatic and metamorphic formations of the Dunhuang Block and its surrounding blocks (Fig. 2; Table 1) allow us to compare the Neoarchean-Paleoproterozoic tectonothermal events of the Dunhuang Block with those of the surrounding blocks. In the Dunhuang Block, there have been recorded two main stages of magmatism of 2.6–2.5 Ga and 2.05–1.80 Ga (Fig. 12). The 2.6–2.5 Ga magmatism mainly corresponds to the

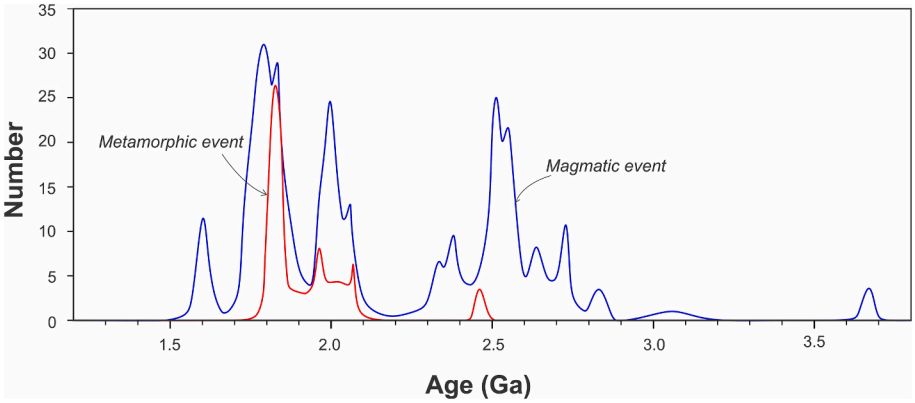


**Fig. 12.** Distribution curves of Neoarchean-Paleoproterozoic magmatic (blue) and metamorphic (red) zircon ages from the Dunhuang Blocks (Table 1).

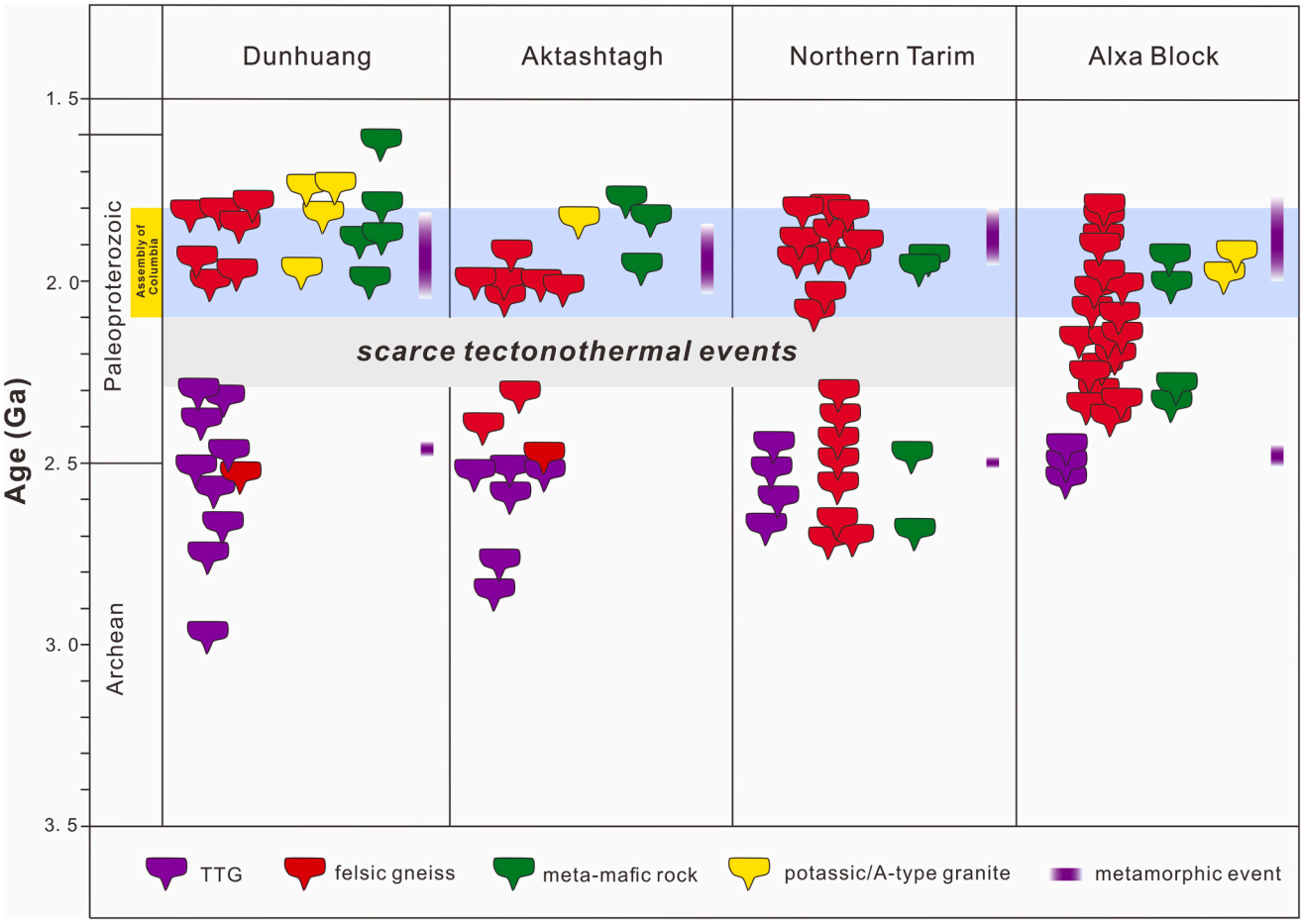


**Fig. 13.** Time-space diagram illustrating Neoarchean-Paleoproterozoic tectonothermal events in the Dunhuang Block (Dunhuang and Aktashtagh regions), northern Tarim Block and Alxa Block. Source: Dunhuang Block – Table 1; northern Tarim Block – Dong et al. (1999); Guo et al. (2003); Hu and Wei (2006); Deng et al. (2008); Long et al. (2010, 2011, 2012); Dong et al. (2011); Shu et al. (2011); Lei et al. (2012); Zhang et al. (2012a); Ge et al. (2013a, 2013b, 2014, 2015); He et al. (2013); Xu et al. (2013); Wu et al. (2020); Alxa Block - Lu (2002); Xiu et al. (2002); Li et al. (2004); Shen et al. (2005); Zhou et al. (2007); Dong et al. (2007); Liu (2008); Geng et al. (2010); Gong et al. (2011, 2012, 2016); Dan et al. (2012); Bao et al. (2013); Zhang et al. (2013a); Wu et al. (2014); Zeng et al. (2018).

emplacement of TTG (Zong et al., 2013; Long et al., 2014; Zhang et al., 2014; Zhao et al., 2015b). During the second stage (2.05–1.80 Ga), mostly felsic rocks with arc geochemical affinities were emplaced (He et al., 2013; Zhu et al., 2018; Diao et al., 2019; Wang et al., 2020; Zhao et al., 2020, 2022). Two episodes of metamorphism have been also recorded in Dunhuang (Fig. 12): an earlier occurred at ~ 2.5 Ga, soon after the crystallization of TTG rocks (Yan et al., 2024), and a later was at 2.05–1.80 Ga (Zhang et al., 2012b, 2013b, 2013; Wang et al., 2013a; Zong et al., 2013; Zhao et al., 2015b; Wu et al., 2019, 2024). In addition, there have been identified two episodes of high pressure granulites-facies metamorphism at ~ 1.97 Ga and ~ 1.85 Ga (Zhang et al., 2012b, 2013b; Wu et al., 2019). A similar succession of Neoarchean-Paleoproterozoic tectonothermal events was recorded in the adjacent northern Tarim and Alxa Block (Fig. 13): (1) ~ 2.5 Ga TTG magmatism and coeval metamorphism; (2) 2.0–1.90 Ga felsic magmatism; (3) 1.95–1.80 Ga high-grade metamorphism. Late Neoarchean (~2.5 Ga) magmatic rocks are exposed in the Kuruktag region of the northern TC and are represented by TTG rocks, granitic gneiss, *meta*-gabbro and *meta*-diorite (Long et al., 2010; Zhang et al., 2012a; Ge et al., 2014). Evidence for the late Paleoproterozoic metamorphism come from supracrustal rocks and migmatites of the Korla Complex in northern Tarim (Ge et al., 2013b, 2014), and from gneisses and TTG rocks of the Longshoushan and Beidashan complexes in the western Alxa Block (Dong et al., 2007; Dan et al., 2012; Zhang et al., 2013a, b; Wu et al., 2014; Gong et al., 2016; Su et al., 2023).

In general, the Neoarchean-Paleoproterozoic tectonothermal events that have been so far documented in the Dunhuang Block are similar to those recorded in the northern Tarim and Alxa blocks, however, the 2.3–2.1 Ga tectonothermal event has not been recorded there (Fig. 13). Thus, the succession of Neoarchean-Paleoproterozoic tectonothermal events in the Dunhuang Block is not the same as in the Alxa Block of the NCC, but more similar to that of the northern Tarim (Fig. 13). Therefore, we consider that the Neoarchean to Paleoproterozoic events of magmatism and metamorphism of the Dunhuang Block should be rather correlated with the Tarim Craton.

Previous studies have shown that the Dunhuang Block and the northern Tarim both keep records of the ca. 2.1–1.8 Ga tectonothermal events that are generally coeval with the global-scale ca. 2.1–1.8 Ga orogeny related to assembly of Columbia supercontinent (e.g., Rogers and Santosh, 2002, 2009; Zhao et al., 2002, 2004; Meert and Santosh, 2017). Therefore, the Dunhuang Block was probably connected with northern Tarim during the assembly of the Columbia supercontinent (Fig. 14; Zhao et al., 2011). The newly discovered ~ 2.04 Ga Dongshuigou amphibolites (this study) and the other *meta*-igneous rocks of the Dunhuang Block, e.g., ~2.05 Ga Hongliuxia dioritic gneisses (Zhao et al., 2022) and ~ 1.99 Ga Sanweishan amphibolites (He et al., 2013), all show arc geochemical affinities and depleted mantle sources as seen in the Hf-in-zircon isotope systematics (Fig. 5). The parental melts of amphibolite magmatic protoliths were likely derived by partial melting of an enriched sub-arc mantle wedge (Fig. 9). The 1.85–1.82 Ga high-

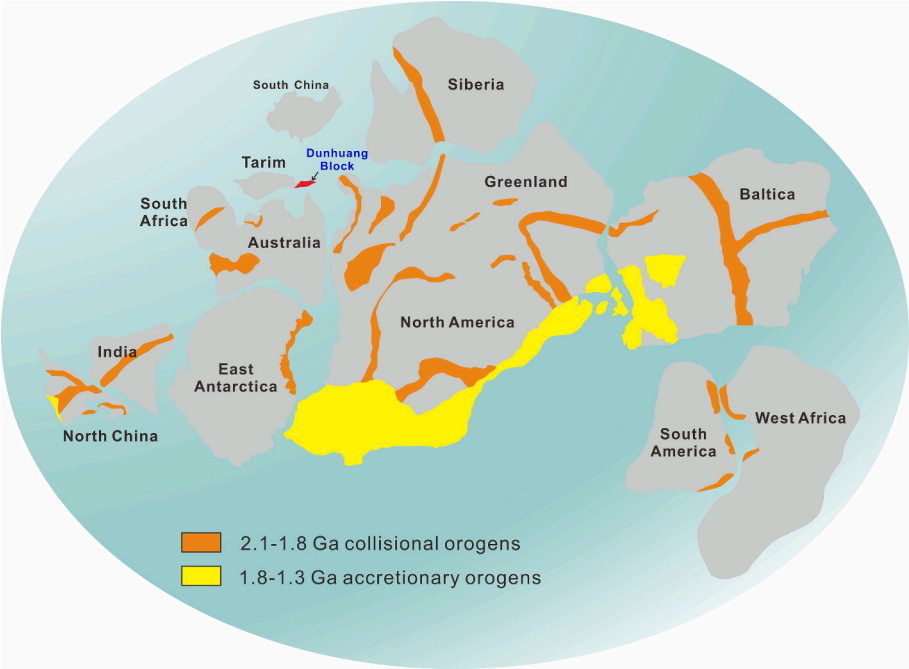


**Fig. 14.** Paleogeographic position of the Dunhuang Block in respect to the Tarim Craton within the Columbia supercontinent (modified after Zhao et al., 2011).

pressure granulites in the Shibaocheng area indicate the beginning of the collisional orogeny (Zhang et al., 2012b, 2013b; Lv et al., 2020). Finally, the occurrence of ~ 1.75 Ga A-type granites in the Huoyanshan area suggests the post-collision stage (Yu et al., 2014; Gan et al., 2020; Lv et al., 2020). A similar succession of Paleoproterozoic tectonothermal events implying a continuous tectonic evolution from subduction to collision orogeny (Xin et al., 2011; Wang et al., 2019; Lv et al., 2020) was also identified in the Aktashtagh region of northern Altyn Tagh (Fig. 13). Evidence for that comes from 2.15–2.0 Ga arc-type gneissic diorite, gneissic granite and gabbro (Xin et al., 2011; Zhang et al., 2014; Zhu et al., 2018) and 2.0–1.85 Ga high-pressure granulite metamorphism (Wu et al., 2019; Zhang et al., 2021). The protoliths of those metamorphic rocks were basement rocks of a Paleoproterozoic magmatic arc (Wu et al., 2019). Subsequently, the 1.87–1.84 Ga massive granites and the mafic dike swarms of Aktashtagh suggest termination of subduction and beginning of post-collisional extension (Wu et al., 2023). Thus, during the Paleoproterozoic, the Dunhuang Block experienced a complete orogenic cycle from oceanic subduction at ca. 2.15–1.90 Ga to subsequent continental collision at ca. 1.85–1.82 Ga and post-collisional extension at ca. 1.79–1.73 Ga.

The subduction-to-collision tectonic model was also suggested in the northern Tarim: an Andean-type continental arc existed during a period of 1.94–1.93 Ga was followed by the late Paleoproterozoic collisional orogeny (Lei et al., 2012; Ma et al., 2013; Ge et al., 2015). Evidence for such an arc and subsequent collisional orogeny comes from Paleoproterozoic granitoids of the Kuruktag area and Korla Complex, both in the northern Tarim, which were emplaced at 1.94–1.93 Ga at an advancing-type accretionary continental margin and then metamorphosed at 1.92–1.91 Ga (Long et al., 2012; Ge et al., 2015) and at ~ 1.85 Ga (Dong et al., 2011; Ge et al., 2013b). Therefore, the Dunhuang Block can be generally correlated with northern Tarim in terms of coeval periods of oceanic subduction and continental collision. Such a continuous subduction-to-collision Paleoproterozoic orogeny that was recorded in both the northern Tarim and Dunhuang blocks, is closely linked to the assembly of the Columbia supercontinent (Figs. 13 and 14).

## 6. Conclusions

The new U-Pb zircon and apatite ages from amphibolites and granitic gneisses of the Dunhuang Block confirmed the crystallization of their magmatic protoliths at 2.02 Ga and 2.04 Ga, respectively, and highlighted two episodes of Paleoproterozoic and late Paleozoic superimposed metamorphism. The amphibolites possessing arc-type geochemical affinities and positive $\varepsilon_{Hf}(t)$ values (+0.71 to + 4.93) were formed by low-degree melting of a mantle wedge source enriched by subduction fluids in a suprasubduction zone setting. The granitic gneisses show TTG-type geochemical affinities, i.e. depleted heavy REE, high Sr/Y (57–82) and $La/Yb_N$ ratios (87–136) and slightly enriched Hf isotopes ($\varepsilon_{Hf}(t)$ = -2.7 to + 1.2) and were produced by melting of TTG-like felsic rocks. The new data confirm that the Dunhuang Block records a succession of Neoarchean-Paleoproterozoic tectonothermal events similar to that of northern Tarim. At ca. 2.0–1.90 Ga, the Dunhuang Block was attached to northern Tarim during the oceanic subduction that was followed by the late Paleoproterozoic collisional orogeny at 1.85–1.82 Ga. Both blocks, Dunhuang and Tarim, were together involved into the assembly of the Columbia supercontinent.

## CRediT authorship contribution statement

**Xiang Ren:** Writing – original draft, Investigation, Formal analysis, Data curation. **Baoping Gan:** Writing – review & editing, Investigation, Funding acquisition, Formal analysis, Data curation. **Inna Safonova:** Writing – review & editing, Supervision, Conceptualization. **Faqiao Li:** Investigation, Formal analysis. **Qingfei Sun:** Methodology, Investigation. **Hongrui Xu:** Investigation, Formal analysis.

## Declaration of competing interest

The authors declare that they have no known competing financial interests or personal relationships that could have appeared to influence the work reported in this paper.

## Acknowledgments

This research was financially supported by the National Natural Science Foundation of China (42302054, W2431031), the China Postdoctoral Science Foundation (2022M712629), and Fundamental Research Funds for the Central Universities (2682022CX029,

2682024CX080). We thank Editor-in-Chief Prof. Jian Zhang for his expeditious editorial handling and helpful suggestions, and we appreciate much two anonymous reviewers for their thoughtful and constructive suggestions and comments that all improved the early version of manuscript greatly.

## Appendix A. Supplementary data

Supplementary data to this article can be found online at https://doi.org/10.1016/j.precamres.2026.108040.

## References


Bao, C., Chen, Y.L., Li, D.P., 2013. LA-ICP-MS zircon U-Pb dating and Hf isotopic compositions of the Paleoproterozoic amphibolite in Bayan Ul area, Inner Mongolia. Geol. Bull. China 32 (10), 1513–1524 in Chinese with English abstract.

Barnes, S.J., 1986. The distribution of chromium among orthopyroxene, spinel and silicate liquid at atmospheric pressure. Geochim. Cosmochim. Acta 50, 1889–1909.

Brenan, J.M., Shaw, H.F., Ryerson, F.J., Phinney, D.L., 1995. Mineral-aqueous fluid partitioning of trace elements at 900 °C and 2.0 GPa: Constraints on the trace element chemistry of mantle and deep crustal fluids. Geochim. Cosmochim. Acta 59, 3331–3350.

Cabanis, B., Lecolle, M., 1989. The La/10-Y/15-Nb/8 diagram: a tool for discrimination volcanic series and evidencing continental crust magmatic mixtures and/or contamination. Comptes Rendus De l'académie Des Sciences 309, 2023–2029.

Che, Z.C., Sun, Y., 1996. The age of the Altun granulite facies complex and the basement of the Tarim Basin. Reg. Geol. China 56, 51–57 in Chinese with English abstract.

Chen, N.S., Liao, F.X., Wang, L., Santosh, M., Sun, M., Wang, Q.Y., Mustafa, H.A., 2013. Late Paleoproterozoic multiple metamorphic events in the Quanji Massif: Links with Tarim and North China Cratons and implications for assembly of the Columbia supercontinent. Precambr. Res. 228, 102–116.

Condie, K.C., 1999. Mafic crustal xenoliths and the origin of the lower continental crust. Lithos 46, 95–101.

Condie, K.C., 2003a. Incompatible element ratios in oceanic basalts and komatiites: Tracking deep mantle sources and continental growth rates with time. Geochem. Geophy. Geosy. 4, 1–28.

Condie, K.C., 2003b. Supercontinents, superplumes and continental growth: the Neoproterozoic record. Geol. Soc. London Spec. Publ. 206, 1–21.

Condie, K.C., 2005. TTGs and adakites: are they both slab melts? Lithos 80, 33–44.

Condie, K.C., 2011. The supercontinent cycle. earth as an evolving planetary system. Academic Press, pp. 317–355.

Corfu, F., Hanchar, J.M., Hoskin, P.W.O., Kinny, P., 2003. Atlas of zircon textures. Rev. Mineral. Geochem. 53, 469–500.

Dan, W., Li, X.H., Guo, J.H., Liu, Y., Wang, X.C., 2012. Paleoproterozoic evolution of the eastern Alxa Block, westernmost North China: evidence from in situ zircon U-Pb dating and Hf-O isotopes. Gondw. Res. 21 (4), 838–864.

Defant, M.J., Drummond, M.S., 1990. Derivation of some modern arc magmas by melting of young subducted lithosphere. Nature 347, 662–665.

Deng, X.L., Shu, L.S., Zhu, W.B., Ma, D.S., Wang, B., 2008. Precambrian tectonism, magmatism, deformation and geochronology of igneous rocks in the Xindi Fault Zone, Xinjiang. Acta Petrol. Sin. 24, 2800–2808 in Chinese with English abstract.

Diao, Z.P., 2018. Timing of formation and its metamorphism and deformation of the Dunhuang complex, Gansu Province. Master's thesis Nanjing University, Nanjing (in Chinese with English abstract).

Diao, Z.P., Zhu, W.B., Wu, H.L., 2019. Metamorphism, deformation and chronological constraints on the Dunhuang complex in Dongbatu area, Dunhuang, Gansu Province. Geol. J. China Universities 25, 144–160 in Chinese with English abstract.

Dong, F.R., Li, S.L., Feng, X.C., 1999. Characteristics of Shengou gneiss complex of Neoarchean from Kuluktag of Xinjiang. Xinjiang Geol. 17, 82–87 in Chinese with English abstract.

Dong, C.Y., Liu, D.Y., Li, J.J., Wang, Y.S., Zhou, H.Y., Li, C.D., Yang, Y.H., Xie, L.W., 2007. Palaeoproterozoic Khondalite Belt in the western North China Craton: New evidence from SHRIMP dating and Hf isotope composition of zircons from metamorphic rocks in the Bayan Ul-Helan Mountains area. Chinese Sci. Bull. 52, 2984–2994.

Dong, X., Zhang, Z.M., Tang, W., 2011. Precambrian tectono-thermal events of the northern margin of the Tarim Craton: constraints of zircon U-Pb chronology from high-grade metamorphic rocks of the Korla, Xinjiang. Acta Petrol. Sin. 27, 47–58 in Chinese with English abstract.

Elliott, T., Plank, T., Zindler, A., White, W., Bourdon, B., 1997. Element transport from slab to volcanic front at the Mariana arc. J. Geophys. Res. Solid Earth 102, 14991–15019.

Evans, D.A.D., Mitchell, R.N., 2011. Assembly and breakup of the core of Paleoproterozoic-Mesoproterozoic supercontinent Nuna. Geology 39, 443–446.

Faure, M., Lin, W., Monie, P., Bruguier, O., 2004. Paleoproterozoic arc magmatism and collision in Liaodong Peninsula (north-east China). Terra Nova 16, 75–80.

Foley, S., Tiepolo, M., Vannuccl, R., 2002. Growth of early continental crust controlled by melting of amphibolite in subduction zones. Nature 417, 837–840.

Gan, B.P., Diwu, C.R., Yan, J.H., Wang, T.Y., Li, J.Y., 2020. Formation and stabilization of the Dunhuang Block, NW China: constraints from the late Paleoproterozoic A-type granites of the Dunhuang complex. Precambr. Res. 346.

Gan, B.P., Tang, J.X., Diwu, C.R., 2024. Magmatism and tectonic evolution at an active continental margin: a case study of the Dunhuang Block. Acta Petrol. Sin. 40, 702–718 in Chinese with English abstract.

Ge, R.F., Zhu, W.B., Wu, H.L., He, J.W., Zheng, B.H., 2013a. Zircon U–Pb ages and Lu–Hf isotopes of Paleoproterozoic metasedimentary rocks in the Korla complex, NW China: implications for metamorphic zircon formation and geological evolution of the Tarim Craton. Precambr. Res. 231, 1–18.

Ge, R.F., Zhu, W.B., Wu, H.L., Zheng, B.H., He, J.W., 2013b. Timing and mechanisms of multiple episodes of migmatization in the Korla complex, northern Tarim Craton, NW China: Constraints from zircon U–Pb–Lu–Hf isotopes and implications for crustal growth. Precambr. Res. 231, 136–156.

Ge, R.F., Zhu, W.B., Wilde, S.A., Wu, H.L., He, J.W., Zheng, B.H., 2014. Archean magmatism and crustal evolution in the northern Tarim Craton: insights from zircon U–Pb–Hf–O isotopes and geochemistry of ~2.7Ga orthogneiss and amphibolite in the Korla complex. Precambr. Res. 252, 145–165.

Ge, R.F., Zhu, W.B., Wilde, S.A., He, J.W., Cui, X., 2015. Synchronous crustal growth and reworking recorded in late Paleoproterozoic granitoids in the northern Tarim craton: in situ zircon U-Pb-Hf-O isotopic and geochemical constraints and tectonic implications. Geol. Soc. Am. Bull. 127, 781–803.

Ge, R.F., Zhu, W.B., Wilde, S.A., Wu, H.L., 2018. Remnants of Eoarchean continental crust derived from a subducted proto-arc. Sci. Adv. 4 (2).

Geng, Y.S., Wang, X.S., Wu, C.M., Zhou, X.W., 2010. Late Paleoproterozoic tectonothermal events of the metamorphic basement in Alxa area: evidence from geochronology. Acta Petrol. Sin. 26 (4), 1159–1170 in Chinese with English abstract.

Gong, J.H., Zhang, J.X., Yu, S.Y., 2011. The origin of Longshoushan Group and associated rocks in the southern part of the Alxa Block: constraints from LA-ICP-MS U-Pb zircon dating. Acta Petrol. Et Mineral. 30 (5), 795–818 in Chinese with English abstract.

Gong, J.H., Zhang, J.X., Yu, S.Y., Li, H.K., Hou, K.J., 2012. Ca. 2.5 Ga TTG rocks in the western Alxa Block and their implications. Chinese Sci. Bull. 57, 4064–4076.

Gong, J.H., Zhang, J.X., Wang, Z.Q., Yu, S.Y., Li, H.K., Li, Y.S., 2016. Origin of the Alxa Block, western China: new evidence from zircon U-Pb geochronology and Hf isotopes of the Longshoushan complex. Gondw. Res. 36, 359–375.

Grove, T.L., Parman, S.W., Bowring, S.A., Price, R.C., Baker, M.B., 2002. The role of an $H_2O$-rich fluid component in the generation of primitive basaltic andesites and andesites from the Mt. Shasta region. N. California. Contrib. Mineral. Petr. 142, 375–396.

Guo, Z.J., Zhang, Z.C., Liu, S.W., Li, H.M., 2003. U-Pb geochronological evidence for the early Precambrian complex of the Tarim Craton, NW China. Acta Petrol. Sin. 19, 537–542 in Chinese with English abstract.

Guo, J.H., Sun, M., Zhai, M.G., 2005. Sm-Nd and SHRIMP U-Pb zircon geochronology of high-pressure granulites in the Sanggan area, North China Craton: timing of Paleoproterozoic continental collision. J. Asian Earth Sci. 24, 629–642.

Guo, J.L., Wu, Y.B., Gao, S., Jin, Z.M., Zong, K.Q., Hu, Z.C., Chen, K., Chen, H.H., Liu, Y. S., 2015. Episodic paleoarchean-paleoproterozoic (3.3-2.0 Ga) granitoid magmatism in Yangtze Craton, South China: Implications for late Archean tectonics. Precambr. Res. 270, 246–266.

Haase, K.M., Goldschmidt, B., Garbe-Schonberg, D., 2004. Petrogenesis of Tertiary continental intra-plate lavas from the Westerwald region. J. Petrol. 45, 883–905.

Hanyu, T., Tatsumi, Y., Nakai, S., Chang, Q., Miyazaki, T., Sato, K., Tani, K., Shibata, T., Yoshida, T., 2006. Contribution of slab melting and slab dehydration to magmatism in the NE Japan arc for the last 25 Myr: Constraints from geochemistry. Geochem. Geophy Geosy 7.

Hawkesworth, C.J., Gallagher, K., Hergt;, J.M., McDermott, F., 1993. Mantle and slab contributions in arc magmas. Annu. Rev. Earth Planet. Sci. 21, 175–204.

He, Z.Y., Zhang, Z.M., Zong, K.Q., Dong, X., 2013. Paleoproterozoic crustal evolution of the Tarim Craton: constrained by zircon U–Pb and Hf isotopes of meta-igneous rocks from Korla and Dunhuang. J. Asian Earth Sci. 78, 54–70.

He, Z.Y., Zhang, Z.M., Zong, K.Q., Dong, X., 2013a. Paleoproterozoic crustal evolution of the Tarim Craton: Constrained by zircon U–Pb and Hf isotopes of meta-igneous rocks from Korla and Dunhuang. J. Asian Earth Sci. 78, 54–70.

He, Z.Y., Zhang, Z.M., Zong, K.Q., Xiang, H., Klemd, R., 2014. Metamorphic P–T–t evolution of mafic HP granulites in the northeastern segment of the Tarim Craton (Dunhuang block): evidence for early Paleozoic continental subduction. Lithos 196–197, 1–13.

Hu, A.Q., Wei, G.J., 2006. On the age of the Neo-Archean Qingir gray gneisses from the Northern Tarim basin Xinjiang, China. Acta Geol. Sin. 80, 126–134 in Chinese with English abstract.

Jourdan, F., Bertrand, H., Scharer, U., Blichert-Toft, J., Feraud, G., Kampunzu, A.B., 2007. Major and trace element and Sr, Nd, Hf, and Pb isotope compositions of the Karoo large igneous province, Botswana-Zimbabwe: Lithosphere vs mantle plume contribution. J. Petrol. 48, 1043–1077.

Kogiso, T., Tatsumi, Y., Nakano, S., 1997. Trace element transport during dehydration processes in the subducted oceanic crust: 1. Experiments and Implications for the origin of ocean island basalts. Earth Planet. Sci. Lett. 148, 193–205.

Lei, R.X., Wu, C.Z., Chi, G.X., Chen, G., Gu, L.X., Jiang, Y.H., 2012. Petrogenesis of the Paleoproterozoic Xishankou pluton, northern Tarim block, northwest China: implications for assembly of the supercontinent Columbia. Int. Geol. Rev. 54, 1829–1842.

Li, X.H., Su, L., Song, B., Liu, D.Y., 2004. SHRIMP U-Pb zircon age of the Jinchuan ultramafic intrusion and its geological significance. Chinese Sci. Bull. 49 (4), 420–422.

Li, Z.X., Evans, D.A.D., Murphy, J.B., 2016a. Supercontinent cycles through earth history. Geol. Soc. London Spec. Publ. 424.

Li, Y.H., Zheng, J.P., Xiong, Q., Wang, W., Ping, X.Q., Li, X.Y., Tang, H.Y., 2016b. Petrogenesis and tectonic implications of Paleoproterozoic metapelitic rocks in the

Archean Kongling complex from the northern Yangtze Craton, South China. Precambr. Res. 276, 158–177.
Liu, Y., 2008. Characteristics and their geological significance of Paleoproterozoic granite in Jinchuan, Gansu Province. Master's degree thesis, Beijing China University of Geoscience (in Chinese with English abstract).
Liu, S.W., Zhao, G.C., Wilde, S.A., Shu, G.M., Sun, M., Li, Q.G., Tian, W., Zhang, J., 2006. Th-U-Pb monazite geochronology of the Lüliang and Wutai Complexes: constraints on the tectonothermal evolution of the Trans-North China Orogen. Precambr. Res. 148, 205–225.
Liu, Y.S., Yu, H.F., Xin, H.T., Lu, S.N., Xiu, Q.Y., Li, Q., 2009. Tectonic units division and Precambrian significant geological events in Altyn Tagh Mountain, China. Geol. Bull. China 28, 1430–1438 in Chinese with English abstract.
Liu, Y.S., Xin, H.T., Zhou, S.J., Teng, X.J., Yang, J.Q., Lv, H.Q., 2010. Precambrian to paleozoic tectonic evolution in the lapeiquan area, eastern altyn tagh. Geological Publishing House, Beijing, p. 211.
Long, X.P., Yuan, C., Sun, M., Zhao, G.C., Xiao, W.J., Wang, Y.J., Yang, Y.H., Hu, A.Q., 2010. Archean crustal evolution of the northern Tarim craton, NW China: Zircon U–Pb and Hf isotopic constraints. Precambr. Res. 180, 272–284.
Long, X.P., Yuan, C., Sun, M., Xiao, W.J., Zhao, G.C., Zhou, K.F., Wang, Y.J., Hu, A.Q., 2011. The discovery of the oldest rocks in the Kuluketage area and its geological implications. Sci. China Earth Sci. 54, 342–348.
Long, X.P., Sun, M., Yuan, C., Kröner, A., Hu, A.Q., 2012. Zircon REE patterns and geochemical characteristics of Paleoproterozoic anatectic granite in the northern Tarim Craton, NW China: implications for the reconstruction of the Columbia supercontinent. Precambr. Res. 222–223, 474–487.
Long, X.P., Yuan, C., Sun, M., Kröner, A., Zhao, G.C., 2014. New geochemical and combined zircon U–Pb and Lu–Hf isotopic data of orthogneisses in the northern Altyn Tagh, northern margin of the Tibetan plateau: Implication for Archean evolution of the Dunhuang Block and crust formation in NW China. Lithos 200–201, 418–431.
Lu, S.N., 2002. Preliminary study of precambrian geology in the north tibet–qinghai plateau. Geological Publishing House, Beijing, p. 125.
Lu, S.N., Yuan, G.B., 2003. Geochronology of early Precambrian magmatic activities in Aktashtagh, East Altyn Tagh. Acta Geol Sin 77, 61–68 in Chinese with English abstract.
Lu, S.N., Li, H.K., Zhang, C.L., Niu, G.H., 2008. Geological and geochronological evidence for the Precambrian evolution of the Tarim Craton and surrounding continental fragments. Precambr. Res. 160, 94–107.
Lv, P., Yu, S.Y., Peng, Y.B., Zhang, J., Xie, W.M., Jiang, X.Z., Gao, X.Y., Ji, W.T., Li, S.Z., Liu, Y.J., 2020. Paleoproterozoic multiple magmatic-metamorphic events in the Dunhuang Block, eastern Tarim Craton: implications for assembly of the Columbia supercontinent. Precambr. Res. 351.
Ma, X.X., Shu, L.S., Santosh, M., Li, J.Y., 2013. Paleoproterozoic collisional orogeny in Central Tianshan: assembling the Tarim Block within the Columbia supercontinent. Precambr. Res. 228, 1–19.
Martin, H., 1986. Effect of steeper Archean geothermal gradient on geochemistry of subduction-zone magmas. Geology 14, 753–756.
Martin, H., 1999. Adakitic magmas: modern analogues of Archaean granitoids. Lithos 411–429.
Martin, H., Smithies, R.H., Rapp, R., Moyen, J.F., Champion, D., 2005. An overview of adakite, tonalite–trondhjemite–granodiorite (TTG), and sanukitoid: relationships and some implications for crustal evolution. Lithos 79, 1–24.
Meert, J.G., Santosh, M., 2017. The Columbia supercontinent revised. Gondw. Res. 50, 67–83.
Mei, H.L., Yu, H.F., Li, Q., Zuo, G.C., 1997. Preliminary litho-tectonic framework of early Precambrian rocks in Dunhuang-Beishan area, Gansu, west China. Progress in Precambr. Res. 20, 47–54 in Chinese with English abstract.
Meng, F.C., Zhang, J.X., Xiang, Z.Q., Yu, S.Y., Li, J.P., 2011. Evolution and formation of the Dunhuang Group in NE Tarim basin, NW China: evidence from detrital zircon geochronology and Hf isotope. Acta Petrol. Sin. 27, 59–76 in Chinese with English abstract.
Meschede, M., 1986. A method of discriminating between different types of mid-ocean ridge basalts and continental tholeiites with the Nb-Zr-Y diagram. Chem. Geol. 56, 207–218.
Middlemost, E.A., 1994. Naming materials in the magma/igneous rock system. Earth Sci. Rev. 37, 215–224.
Mitchell, R.N., Zhang, N., Salminen, J., Liu, Y.B., Spencer, C.J., Steinberger, B., Murphy, J.B., Li, Z.X., 2021. The supercontinent cycle. Nat. Rev. Earth Env. 2, 358–374.
Miyashiro, A., 1974. Volcanic rocks series in island arcs and active continental margins. Am. J. Sci. 174, 321–355.
Moyen, J.F., Martin, H., 2012. Forty years of TTG research. Lithos 148, 312–336.
Mungall, J.E., 2007. Crustal contamination of picritic magmas during transport through dikes: the expo intrusive suite, cape smith fold belt, New Quebec. J. Petrol. 48, 1021–1039.
Murphy, J.B., Nance, R.D., 2013. Speculations on the mechanisms for the formation and breakup of supercontinents. Geosci. Front. 4, 185–194.
Nabelek, P.I., 1980. Nickel partitioning between olivine and liquid in natural basalts: henry's law behavior. Earth Planet. Sci. Lett. 48, 293–302.
Nance, R.D., Murphy, J.B., Santosh, M., 2014. The supercontinent cycle: a retrospective essay. Gondw. Res. 25, 4–29.
Palin, R.M., White, R.W., Green, E.C.R., 2016. Partial melting of metabasic rocks and the generation of tonalitic–trondhjemitic–granodioritic (TTG) crust in the Archaean: constraints from phase equilibrium modelling. Precambr. Res. 287, 73–90.
Patiño Douce, A.E., 2005. Vapor-absent melting of tonalite at 15-32 kbar. J. Petrol. 46, 275–290.
Pearce, J.A., 2008. Geochemical fingerprinting of oceanic basalts with applications to ophiolite classification and the search for Archean oceanic crust. Lithos 100, 14–48.
Peccerillo, A., Taylor, S.R., 1976. Geochemistry of Eocene calc-alkaline volcanic rocks from the Kastamonu area, Northern Turkey: Contrib. Mineral. Petr. 58, 63–81.
Plank, T., 2005. Constraints from Thorium/Lanthanum on sediment recycling at subduction zones and the evolution of the continents. J. Petrol. 46, 921–944.
Plank, T., Langmuir, C.H., 1998. The chemical composition of subducting sediment and its consequences for the crust and mantle. Chem. Geol. 145, 325–394.
Rapp, R.P., Watson, E.B., 1995. Dehydration melting of metabasalt at 8-32 kbar: Implications for continental growth and crust-mantle recycling. J. Petrol. 36, 891–931.
Rapp, R.P., Watson, E.B., Miller, C.F., 1991. Partial melting of amphibolite/eclogite and the origin of Archean trondhjemites and tonalites. Precambr. Res. 51, 1–25.
Rapp, R.P., Shimizu, N., Norman, M.D., Applegate, G.S., 1999. Reaction between slab-derived melts and peridotite in the mantle wedge: experimental constraints at 3.8 GPa. Chem. Geol. 160, 335–356.
Rapp, R.P., Schimizu, N., Norman, M.D., 2003. Growth of early continental crust by partial melting of eclogite. Nature 425, 605–609.
Rapp, R.P., Norman, M.D., Laporte, D., Yaxley, G.M., Martin, H., Foley, S.F., 2010. Continent formation in the Archean and chemical evolution of the cratonic lithosphere: melt-rock reaction experiments at 3-4 GPa and petrogenesis of Archean mg-diorites (sanukitoids). J. Petrol. 51, 1237–1266.
Rogers, J.J.W., Santosh, M., 2002. Configuration of Columbia, a Mesoproterozoic supercontinent. Gondw. Res. 5, 5–22.
Rogers, J.J.W., Santosh, M., 2009. Tectonics and surface effects of the supercontinent Columbia. Gondw. Res. 15, 373–380.
Roux, V.L., Dasgupta, R., Lee, C.T.A., 2011. Mineralogical heterogeneities in the Earth's mantle: constraints from Mn, Co, Ni and Zn partitioning during partial meltin. Earth Planet. Sci. Lett. 307, 395–408.
Rudnick, R.L., 1995. Making continental crust. Nature 378, 571–577.
Rudnick, R.L., Gao, S., 2003. Composition of the continental crust. Treatise on Geochemistry Elsevier 3, 1–64.
Sato, H., 1977. Nickel content of basaltic magmas: identification of primary magmas and a measure of the degree of olivine fractionation. Lithos 10, 113–120.
Schmidt, M.W., Jagoutz, O., 2017. The global systematics of primitive arc melts. Geochem. Geophy. Geosy. 18, 2817–2854.
Sen, C., Dunn, T., 1994. Dehydration melting of a basaltic composition amphibolite at 1.5 and 2.0 GPa: implications for the origin of adakites. Contrib. Mineral. Petr. 117, 394–409.
Shen, Q.H., Geng, Y.S., Wang, X.S., Wu, C.M., 2005. Petrology, geochemistry, formation environment and ages of Precambrian amphibolites in Alxa region. Acta Petrol. Et Mineral. 24 (1), 21–31 in Chinese with English abstract.
Shervais, J.W., 1982. Ti-V plots and the petrogenesis of modern and ophiolitic lavas. Earth Planet. Sci. Lett. 59, 101–118.
Shu, L.S., Deng, X.L., Zhu, W.B., Ma, D.S., Xiao, W.J., 2011. Precambrian tectonic evolution of the Tarim block, NW China: new geochronological insights from the Quruqtagh domain. J. Asian Earth Sci. 42, 774–790.
Si, Y., Ge, R.F., Zhou, T., Wang, Y., 2022. Decoupling of metamorphic zircon U-Pb ages and P-T paths in the Dunhuang metamorphic complex, Northwestern China. Precambr. Res. 379.
Skjerlie, K.P., Patiño-Douce, A.E., 2002. The fluid-absent partial melting of a zoisite-bearing quartz eclogite from 1·0 to 3·2 GPa; implications for melting in thickened continental crust and for subduction-zone processes. J. Petrol. 43, 291–314.
Smithies, R.H., 2000. The Archaean tonalite-trondhjemite-granodiorite (TTG) series is not an analogue of Cenozoic adakite. Earth Planet. Sci. Lett. 182, 115–125.
Smithies, R.H., Champion, D.C., Van Kranendonk, M.J., 2009. Formation of Paleoarchean continental crust through infracrustal melting of enriched basalt. Earth Planet. Sci. Lett. 281, 298–306.
Spandler, C., Pirard, C., 2013. Element recycling from subducting slabs to arc crust: a review. Lithos 170–171, 208–223.
Stern, C.R., Kilian, R., 1996. Role of the subducted slab, mantle wedge and continental crust in the generation of adakites from the Austral Volcanic Zone. Contrib. Mineral. Petr. 123, 263–281.
Su, W.H., Wang, Q., Kang, J., Song, X.Y., 2023. Proterozoic evolution of the Alxa block in western China: a wandering terrane during supercontinent cycles. Precambr. Res. 389.
Sun, S.S., McDonough, W.S., 1989. Chemical and isotopic systematics of oceanic basalts: implications for mantle composition and processes. Geol. Soc. London Spec. Publ. 42, 313–345.
Tatsumi, Y., Eggins, S.M., 1995. Subduction zone magmatism. Blackwell Science, Cambridge, MA.
Tatsumi, Y., Hamilton, D.L., Nesbitt, R.W., 1986. Chemical characteristics of fluid phase released from a subducted lithosphere and origin of arc magmas: evidence from high-pressure experiments and natural rocks. J. Volcanol. Geoth. Res. 29, 293–309.
Wan, Y.S., Liu, S.J., Xie, H.Q., Dong, C.Y., Li, Y., Bai, W.Q., Liu, D.Y., 2018. Formation and evolution of the Archean continental crust of China: a review. China Geol. 1, 109–136.
Wang, Q., Wyman, D.A., Xu, J.F., Jian, P., Zhao, Z.H., Li, C.F., Xu, W., Ma, J.L., He, B., 2007. Early cretaceous adakitic granites in the Northern Dabie complex, central China: implications for partial melting and delamination of thickened lower crust. Geochim. Cosmochim. Acta 71, 2609–2636.
Wang, J., Wu, Y.B., Gao, S., Peng, M., Liu, X.C., Zhao, L.S., Zhou, L., Hu, Z.C., Gong, H.J., Liu, Y.S., 2010. Zircon U-Pb and trace element data from rocks of the Huai'an complex: new insights into the late Paleoproterozoic collision between the Eastern and Western Blocks of the North China Craton. Precambr. Res. 178, 59–71.

Wang, Z.M., Han, C.M., Su, B.X., Sakyi, P.A., Malaviarachchi, S.P.K., Ao, S.J., Wang, L.J., 2013a. The metasedimentary rocks from the eastern margin of the Tarim Craton: petrology, geochemistry, zircon U–Pb dating, Hf isotopes and tectonic implications. Lithos 179, 120–136.
Wang, Z.M., Xiao, W.J., Han, C.M., Ao, S.J., Wang, L.J., 2013b. Metamorphism, zircon U-Pb dating and tectonic implications of garnet amphibolites from Hongliuxia, Dunhuang, Gansu Province. Acta Petrol. Sin. 29, 1685–1697 in Chinese with English abstract.
Wang, W., Zhou, M.F., Zhao, X.F., Chen, W.T., Yan, D.P., 2014a. Late Paleoproterozoic to Mesoproterozoic rift successions in SW China: implication for the Yangtze Block-North Australia-Northwest Laurentia connection in the Columbia supercontinent. Sed. Geol. 309, 33–47.
Wang, Z.M., Han, C.M., Xiao, W.J., Wan, B., Sakyi, P.A., Ao, S.J., Zhang, J.E., Song, D.F., 2014b. Petrology and geochronology of Paleoproterozoic garnet-bearing amphibolites from the Dunhuang Block, Eastern Tarim Craton. Precambr. Res. 255, 163–180.
Wang, H.Y.C., Chen, H.X., Lu, J.S., Wang, G.D., Peng, T., Zhang, H.C.G., Yan, Q.R., Hou, Q.L., Zhang, Q., Wu, C.M., 2016. Metamorphic evolution and SIMS U-Pb geochronology of the Qingshigou area, Dunhuang block, NW China: tectonic implications of the southernmost Central asian orogenic belt. Lithosphere 8, 463–479.
Wang, H.Y.C., Chen, H.X., Zhang, Q.W.L., Shi, M.Y., Yan, Q.R., Hou, Q.L., Zhang, Q., Kusky, T., Wu, C.M., 2017a. Tectonic mélange records the Silurian–Devonian subduction-metamorphic process of the southern Dunhuang terrane, southernmost Central Asian Orogenic Belt. Geology 45, 427–430.
Wang, H.Y.C., Wang, J., Wang, G.D., Lu, J.S., Chen, H.X., Peng, T., Zhang, H.C.G., Zhang, Q.W.L., Xiao, W.J., Hou, Q.L., Yan, Q.R., Zhang, Q., Wu, C.M., 2017b. Metamorphic evolution and geochronology of the Dunhuang orogenic belt in the Hongliuxia area, Northwestern China. J. Asian Earth Sci. 135, 51–69.
Wang, Z.M., Han, C.M., Xiao, W.J., Su, B.X., Ding, J.X., 2017c. Paleoproterozoic subduction-related magmatism and crustal evolution of the Dunhuang Block, NW China. J. Asian Earth Sci. 134, 13–28.
Wang, H.Y.C., Zhang, Q.W.L., Lu, J.S., Chen, H.X., Liu, J.H., Zhang, H.C.G., Pham, V.T., Peng, T., Wu, C.M., 2018. Metamorphic evolution and geochronology of the tectonic mélange of the Dongbatu and Mogutai blocks, middle Dunhuang orogenic belt, Northwestern China. Geosphere 14, 883–906.
Wang, Z.M., Han, C.M., Xiao, W.J., Asamoah Sakyi, P., Yang, L., Zhao, N., 2019. Mineralogy, geochemistry, and zircon U-Pb-Hf isotopes of the Paleoproterozoic granulite-facies metamorphic rocks from the Aktashtagh region, southeastern Tarim Craton. Precambr. Res. 321, 13–33.
Wang, Z.M., Han, C.M., Xiao, W.J., Asamoah Sakyi, P., 2020. Paleoproterozoic multiphase magmatism and metamorphism recorded in metamorphic basement rocks of the northern Altyn Tagh, southeastern Tarim Craton. Precambr. Res. 346.
Whitney, D.L., Evans, B.W., 2010. Abbreviations for names of rock-formation minerals. Am. Mineral. 95, 185–187.
Wilde, S.A., Zhao, G.C., Sun, M., 2002. Development of the North China Craton during the late Archean and its final amalgamation at 1.8 Ga: some speculations on its position within a global Paleoproterozoic supercontinent. Gondw. Res. 5, 85–94.
Winchester, J.A., 1984. The geochemistry of the Strathconon amphibolites, Northern Scotland. Scot. J. Geol. 20, 37–51.
Winchester, J.A., Floyd, P.A., 1977. Geochemical discrimination of different magma series and their differentiation products using immobile elements. Chem. Geol. 20, 325–343.
Wood, D.A., 1980. The application of a Th-Hf-Ta diagram to problems of tectonomagmatic classification and to establishing the nature of crustal contamination of basaltic lavas of the British Tertiary Volcanic Province. Earth Planet. Sci. Lett. 50, 11–30.
Wooden, J.L., Czamanske, G.K., Fedorenko, V.A., Arndt, N.T., Chauvel, C., Bouse, R.M., King, B.S.W., Knight, R.J., Siems, D.F., 1993. Isotopic and trace-element constraints on mantle and crustal contributions to Siberian continental flood basalts, Noril'sk area, Siberia. Geochim. Cosmochim. Acta 57, 3677–3704.
Woodhead, J.D., Hergt;, J.M., Davidson, J.P., Eggins, S.M., 2001. Hafnium isotope evidence for "conservative" element mobility during subduction zone processes. Earth Planet. Sci. Lett. 192, 331–346.
Wu, Y.B., Gao, S., Gong, H.J., Xiang, H., Jiao, W.F., Yang, S.H., Liu, Y.S., Yuan, H.L., 2009. Zircon U-Pb age, trace element and Hf isotope composition of Kongling terrane in the Yangtze Craton: refining the timing of Paleoproterozoic high-grade metamorphism. J. Metam. Geol. 27, 461–477.
Wu, S.J., Hu, J.M., Ren, M.H., Gong, W.B., Liu, Y., Yan, J.Y., 2014. Petrography and zircon U-Pb isotopic study of the Bayanwulashan complex: constraints on the Paleoproterozoic evolution of the Alxa Block, westernmost North China Craton. J. Asian Earth Sci. 94, 226–239.
Wu, H.L., Zhu, W.B., Ge, R.F., 2019. Late Paleoproterozoic granulite-facies metamorphism in the North Altyn Tagh area, southeastern Tarim craton: pressure-temperature paths, zircon U-Pb ages, and tectonic implications. Geol. Soc. Am. Bull. 131, 1591–1606.
Wu, G.H., Yang, S., Meert, J.G., Xiao, Y., Chen, Y.Q., Wang, Z.C., Li, X., 2020. Two phases of Paleoproterozoic orogenesis in the Tarim Craton: implications for Columbia assembly. Gondw. Res. 83, 201–216.
Wu, H.L., Zhu, W.B., Ge, R.F., 2024. Garnet growth and diffusion zoning during the late Paleoproterozoic metamorphism, North Altyn area, SE Tarim Craton, NW China: implications for a long-lived hot orogen. Geol. Soc. Am. Bull. 136, 557–582.
Xin, H.T., Zhao, F.Q., Luo, Z.H., Liu, Y.S., Wan, Y.S., Wang, S.Q., 2011. Determination of the Paleoproterozoic geochronological framework in Aqtashtagh area in southeastern Tarim, China, and its geological significance. Acta Geol. Sin. 85, 1977–1993 in Chinese with English abstract.
Xin, H.T., Liu, Y.S., Luo, Z.H., Song, S.C., Wang, S.Q., 2013. The growth of Archean continental crust in Aqtashtagh area of southeast Tarim, China: constraints from petrochemistry and chronology about Milan Group and TTG-gneiss. Earth Sci. Front. 20, 240–259 in Chinese with English abstract.
Xiu, Q.Y., Lu, S.N., Yu, H.F., Yang, C.L., 2002. The isotopic age evidence for main Longshoushan Group contributing to Paleoproterozoic. Prog. Precambr. Res. 25 (2), 93–96 in Chinese with English abstract.
Xu, Z.Q., He, B.Z., Zhang, C.L., Zhang, J.X., Wang, Z.M., Cai, Z.H., 2013. Tectonic framework and crustal evolution of the Precambrian basement of the Tarim Block in NW China: new geochronological evidence from deep drilling samples. Precambr. Res. 235, 150–162.
Yan, J.H., 2017. Formation and evolution of the Dunhuang block: Evidence from the Archean-Paleozoic rocks in Dongbatu area. Master's thesis, Northwest University, Xi'an (in Chinese with English abstract).
Yan, J.H., Gan, B.P., Diwu, C.R., Wang, T.Y., 2024. Late Neoarchean magmatism and tectono-thermal events in the Dunhuang Block, NW China: evidence from TTG gneisses of the Dongbatu Mountains area. Acta Petrol. Sin. 40 (11), 3484–3505 in Chinese with English abstract.
Yin, C.Q., Lin, S.F., Davis, D.W., Zhao, G.C., Xiao, W.J., Li, L.M., He, Y.H., 2013. 2.1-1.85 Ga tectonic events in the Yangtze Block, South China: petrological and geochronological evidence from the Kongling complex and implications for the reconstruction of supercontinent Columbia. Lithos 182–183, 200–210.
Yu, S.Y., Zhang, J.X., Zhao, X.L., Gong, J.H., Li, Y.S., 2014. Geochronology, geochemistry and petrogenesis of the late Paleoproterozoic A-type granites from the Dunhuang block, SE Tarim Craton, China: implications for the break-up of the Columbia supercontinent. Geol. Mag. 151, 629–648.
Zeng, R.Y., Lai, J.Q., Mao, X.C., Li, B., Zhang, J.D., Bayless, R.C., Yang, L.Z., 2018. Paleoproterozoic multiple tectonothermal events in the Longshoushan area, Western North China Craton and their geological implication: evidence from geochemistry, zircon U-Pb geochronology and Hf isotopes. Minerals 8.
Zhai, M.G., Liu, W.J., 2003. Paleoproterozoic tectonic history of the north China Craton: a review. Precambr. Res. 122, 183–199.
Zhai, M.G., Santosh, M., 2011. The early Precambrian odyssey of North China Craton: a synoptic overview. Gondw. Res. 20, 6–25.
Zhai, M.G., Li, T.S., Peng, P., Hu, B., Liu, F., Zhang, Y.B., Guo, J.H., 2010. Precambrian key tectonic events and evolution of the North China Craton. In Kusky, T.M., Zhai, M.G., Xiao, W.J. (Eds.), The Evolving Continents. Geol. Soc. London, Spec. Publ. 338, 235–262.
Zhang, S.B., Zheng, Y.F., Wu, Y.B., Zhao, Z.F., Gao, S., Wu, F.Y., 2006. Zircon U-Pb age and Hf-O isotope evidence for Paleoproterozoic metamorphic event in South China. Precambr. Res. 151, 265–288.
Zhang, J.X., Li, H.K., Meng, F.C., Xiang, Z.Q., Yu, S.Y., Li, J.P., 2011. Polyphase tectonothermal events recorded in "metamorphic basement" from the Altyn Tagh, the southeastern margin of the Tarim basin, western China: constraint from zircon U-Pb geochronology. Acta Petrol. Sin. 27, 23–46 in Chinese with English abstract.
Zhang, C.L., Li, H.K., Santosh, M., Li, Z.X., Zou, H.B., Wang, H.Y., Ye, H.M., 2012a. Precambrian evolution and cratonization of the Tarim Block, NW China: petrology, geochemistry, Nd-isotopes and U-Pb zircon geochronology from Archean gabbro-TTG-potassic granite suite and Paleoproterozoic metamorphic belt. J. Asian Earth Sci. 47, 5–20.
Zhang, J.X., Gong, J.H., Yu, S.Y., 2012b. 1.85 Ga HP granulite-facies metamorphism in the Dunhuang block of the Tarim Craton, NW China: evidence from U–Pb zircon dating of mafic granulites. J. Geol. Soc. 169, 511–514.
Zhang, J.X., Gong, J.H., Yu, S.Y., Li, H.K., Hou, K.J., 2013a. Neoarchean–Paleoproterozoic multiple tectonothermal events in the western Alxa block, North China Craton and their geological implication: evidence from zircon U–Pb ages and Hf isotopic composition. Precambr. Res. 235, 36–57.
Zhang, J.X., Yu, S.Y., Gong, J.H., Li, H.K., Hou, K.J., 2013b. The latest Neoarchean–Paleoproterozoic evolution of the Dunhuang block, eastern Tarim craton, northwestern China: evidence from zircon U–Pb dating and Hf isotopic analyses. Precambr. Res. 226, 21–42.
Zhang, C.L., Zou, H.B., Santosh, M., Ye, X.T., Li, H.K., 2014. Is the Precambrian basement of the Tarim Craton in NW China composed of discrete terranes? Precambr. Res. 254, 226–244.
Zhang, Q.W.L., Liu, J.H., Wang, H.Y.C., Shi, M.Y., Chen, Y.C., Li, Z.M.G., Zhang, H.C.G., Pham, V.T., Wu, C.M., 2019. Amphibolite facies metamorphism and geochronology of the Paleoproterozoic Aktashtagh Orogenic Belt, northwestern China. Precambr. Res. 328, 146–160.
Zhang, Q.W.L., Li, Z.M.G., Shi, M.Y., Chen, Y.C., Liu, J.H., Wu, C.M., 2021. $^{40}Ar/^{39}Ar$ dating of hornblende and U-Pb dating of zircon in the Aktashtagh orogen, NW China: constraints on exhumation and cooling in the Paleoproterozoic. Precambr. Res. 352.
Zhao, Y., 2017. Composition and evolution of the Dunhuang orogenic belt. Doctor's dissertation Northwest University, Xi'an (in Chinese with English abstract).
Zhao, G.C., Cawood, P.A., 2012. Precambrian geology of china. Precambr. Res. 222–223, 13–54.
Zhao, G.C., Zhai, M.G., 2013. Lithotectonic elements of Precambrian basement in the North China Craton: review and tectonic implications. Gondw. Res. 23, 1207–1240.
Zhao, G.C., Cawood, P.A., Wilde, S.A., Sun, M., 2002. Review of global 2.1–1.8 Ga orogens: implications for a pre-Rodinia supercontinent. Earth Sci. Rev. 59, 125–162.
Zhao, G.C., Sun, M., Wilde, S.A., Li, S.Z., 2003. Assembly, accretion and breakup of the Paleo-Mesoproterozoic Columbia supercontinent: records in the North China Craton. Gondw. Res. 6, 417–434.
Zhao, G.C., Sun, M., Wilde, S.A., Li, S.Z., 2004. A Paleo-Mesoproterozoic supercontinent: assembly, growth and breakup. Earth Sci. Rev. 67, 91–123.

Zhao, G.C., Sun, M., Wilde, S.A., Li, S.Z., 2005. Late Archean to Paleoproterozoic evolution of the North China Craton: key issues revisited. Precambr. Res. 136, 177–202.
Zhao, G.C., Li, S.Z., Sun, M., Wilde, S.A., 2011. Assembly, accretion, and break-up of the Palaeo-Mesoproterozoic Columbia supercontinent: record in the North China Craton revisited. Int. Geol. Rev. 53, 1331–1356.
Zhao, G.C., Cawood, P.A., Li, S.Z., Wilde, S.A., Sun, M., Zhang, J., He, Y.H., Yin, C.Q., 2012. Amalgamation of the North China Craton: key issues and discussion. Precambr. Res. 222–223, 55–76.
Zhao, Y., Diwu, C.R., Sun, Y., Zhu, T., Wang, H.L., 2013. Zircon geochronology and Lu-Hf isotope compositions for Precambrian rocks of the Dunhuang complex in Shuixiakou area, Gansu Province. Acta Petrol. Sin. 29, 1698–1712 in Chinese with English abstract.
Zhao, Y., Diwu, C.R., Ao, W.H., Wang, H.L., Zhu, T., Sun, Y., 2015a. Ca. 3.06 Ga granodioritic gneiss in Dunhuang block. Chinese Sci. Bull. 60, 75–87 in Chinese with English abstract.
Zhao, Y., Sun, Y., Yan, J.H., Diwu, C.R., 2015b. The Archean-Paleoproterozoic crustal evolution in the Dunhuang region, NW China: Constraints from zircon U–Pb geochronology and in situ Hf isotopes. Precambr. Res. 271, 83–97.
Zhao, Y., Sun, Y., Diwu, C.R., Guo, A.L., Ao, W.H., Zhu, T., 2016. The dunhuang block is a paleozoic orogenic belt and part of the Central Asian Orogenic Belt (CAOB), NW China. Gondwana Res. 30, 207–223.
Zhao, Y., Ao, W.H., Zhang, H., Wang, Q., Zhai, M.G., Sun, Y., 2019a. Latest Paleoproterozoic (ca. 1.8-1.6 Ga) extensional tectonic setting in the Dunhuang terrane, NW China: evidence from geochronological and geochemical investigations on A-type granite and metamafic rock. Lithosphere 11 (6), 834–854.
Zhao, Y., Sun, Y., Ao, W.H., Zhang, H., Zhu, T., 2019b. Depositional age, provenance and tectonic significance of Precambrian metasedimentary rocks from the Dunhuang complex, NW China: evidence from field investigation, zircon U–Pb geochronology and whole–rock geochemistry. Precambr. Res. 326, 272–294.
Zhao, Y., Ao, W.H., Zhang, H., Wang, Q., 2020. Possible imprints of late Paleoproterozoic orogeny in the Dunhuang terrane, NW China: constraints from igneous and metapelitic rocks. Precambr. Res. 350.
Zhao, Y., Ao, W.H., Zhu, T., Hu, Y.H., Tian, Z.B., Zhang, R.Y., Zhao, J., 2022. Paleoproterozoic (ca. 2.1–1.9 Ga) dioritic-granitic magmatism in the Dunhuang Terrane, Northwestern China: implications for petrogenesis and tectonic evolution. Lithos 432–433.
Zhou, H.Y., Mo, X.X., Li, J.J., Li, H.M., 2007. The U-Pb isotopic dating age of single zircon from biotite plagioclase gneiss in the Qinggele area, Alashan, W-estern Inner Mongolia. Bulletin of Mineralogy, Petrol. Geochem. 26 (3), 221–223 in Chinese with English abstract.
Zhou, X.W., Zhao, G.C., Wei, C.J., Geng, Y.S., Sun, M., 2008. Metamorphic evolution and Th-U-Pb zircon and monazite geochronology of high-pressure pelitic granulites in the Jiaobei massif of the North China Craton. Am. J. Sci. 308, 328–350.
Zhu, W.B., Ge, R.F., Wu, H.L., 2018. Paleoproterozoic ca. 2.0 Ga magmatic-metamorphic event in the northern Altyn Tagh area. Acta Petrol. Sin. 34, 1175–1190 in Chinese with English abstract.
Zong, K.Q., Zhang, Z.M., He, Z.Y., Hu, Z.C., Santosh, M., Liu, Y.S., Wang, W., 2012. Early Palaeozoic high-pressure granulites from the Dunhuang block, northeastern Tarim Craton: constraints on continental collision in the southern Central Asian Orogenic Belt. J. Metam. Geol. 30, 753–768.
Zong, K.Q., Liu, Y.S., Zhang, Z.M., He, Z.Y., Hu, Z.C., Guo, J.L., Chen, K., 2013. The generation and evolution of Archean continental crust in the Dunhuang block, northeastern Tarim craton, Northwestern China. Precambr. Res. 235, 251–263.